AGU PUBLICATIONS

Geochemistry, Geophysics, Geosystems

RESEARCH ARTICLE
10.1002/2014GC005387

Special Section:
Assessing Magmatic, Neovolcanic, Hydrothermal, and Biological Processes along Intra-Oceanic Arcs and Back-Arcs

Eruptive modes and hiatus of volcanism at West Mata seamount, NE Lau basin: 1996–2012

Robert W. Embley[1], Susan G. Merle[2], Edward T. Baker[3], Kenneth H. Rubin[4], John E. Lupton[1], Joseph A. Resing[5], Robert P. Dziak[2], Marvin D. Lilley[6], William W. Chadwick Jr.[2], T. Shank[7], Ron Greene[2], Sharon L. Walker[4], Joseph Haxel[2], Eric Olson[6], and Tamara Baumberger[8,9]

[1]NOAA Pacific Marine Environmental Laboratory, Newport, Oregon, USA, [2]Cooperative Institute of Marine Resources Studies, Oregon State University and NOAA PMEL, Newport, Oregon, USA, [3]NOAA Pacific Marine Environmental Laboratory, Seattle, Washington, USA, [4]SOEST, University of Hawaii at Manoa, Honolulu, Hawaii, USA, [5]Joint Institute for the Study of the Atmospheres and Oceans, University of Washington and NOAA PMEL, Seattle, Washington, USA, [6]School of Oceanography, University of Washington, Seattle, Washington, USA, [7]Woods Hole Oceanographic Institution, Woods Hole, Massachusetts, USA, [8]Centre for Geobiology and Department of Earth Science, University of Bergen, Bergen, Norway, [9]Department of Earth Sciences, ETH Zurich, Zurich, Switzerland

Abstract We present multiple lines of evidence for years to decade-long changes in the location and character of volcanic activity at West Mata seamount in the NE Lau basin over a 16 year period, and a hiatus in summit eruptions from early 2011 to at least September 2012. Boninite lava and pyroclasts were observed erupting from its summit in 2009, and hydroacoustic data from a succession of hydrophones moored nearby show near-continuous eruptive activity from January 2009 to early 2011. Successive differencing of seven multibeam bathymetric surveys of the volcano made in the 1996–2012 period reveals a pattern of extended constructional volcanism on the summit and northwest flank punctuated by eruptions along the volcano's WSW rift zone (WSWRZ). Away from the summit, the volumetrically largest eruption during the observational period occurred between May 2010 and November 2011 at ~2920 m depth near the base of the WSWRZ. The (nearly) equally long ENE rift zone did not experience any volcanic activity during the 1996–2012 period. The cessation of summit volcanism recorded on the moored hydrophone was accompanied or followed by the formation of a small summit crater and a landslide on the eastern flank. Water column sensors, analysis of gas samples in the overlying hydrothermal plume and dives with a remotely operated vehicle in September 2012 confirmed that the summit eruption had ceased. Based on the historical eruption rates calculated using the bathymetric differencing technique, the volcano could be as young as several thousand years.

Key Points:
- Unprecedented study of evolution of boninitic submarine volcano over 16 years
- Eruptive activity in 1996–2010 period occurred both at summit and on rift zone
- Hiatus in eruptive activity beginning in late 2010 or early 2011

Supporting Information:
- Readme S1–S3
- Figures S1–S3
- Tables S1–S4

Correspondence to:
R. W. Embley,
robert.w.embley@noaa.gov

Citation:
Embley, R. W., et al. (2014), Eruptive modes and hiatus of volcanism at West Mata seamount, NE Lau basin: 1996–2012, *Geochem. Geophys. Geosyst.*, *15*, 4093–4115, doi:10.1002/2014GC005387.

Received 23 APR 2014
Accepted 30 SEP 2014
Accepted article online 6 OCT 2014
Published online 31 OCT 2014

1. Introduction and Background

Over the past three decades, thousands of seamounts (most of which are submarine volcanoes) have been mapped with multibeam bathymetric sonars, revealing their accurate locations and first and second-order features such as craters, cones, calderas, syneruptive and posteruptive faults, and their relationship to regional tectonic features. Because most of these submarine volcanoes are extinct [*Staudigel and Clague*, 2010], we lack information on their formation and change over time. One approach to learning about the geologic evolution of seamounts is careful in situ and temporal studies of young submarine volcanoes that lie near or along the Mid-Ocean Ridge, at oceanic hotspots, and within submarine arc and back-arc basins. Many of these volcanoes will continue to evolve geologically as a result of active magmatism and tectonism. On land, we monitor most active volcanoes using remote sensing, seismological, and geodetic techniques, and can usually relate major changes in their morphology to eruptive episodes, but quantifying changes induced during active submarine volcanism is considerably more difficult [*Rubin et al.*, 2012].

Characterization of submarine volcanic eruptions has most often resulted from serendipitous discovery and/or careful field mapping, as in cases reviewed in *Rubin et al.* [2012] or, more rarely, from monitoring combined with posteruptive in situ studies and high-resolution near-bottom acoustic mapping [*Caress et al.*, 2012; *Chadwick et al.*, 2012a; *Dziak et al.*, 2012; *Fornari et al.*, 2012]. Direct

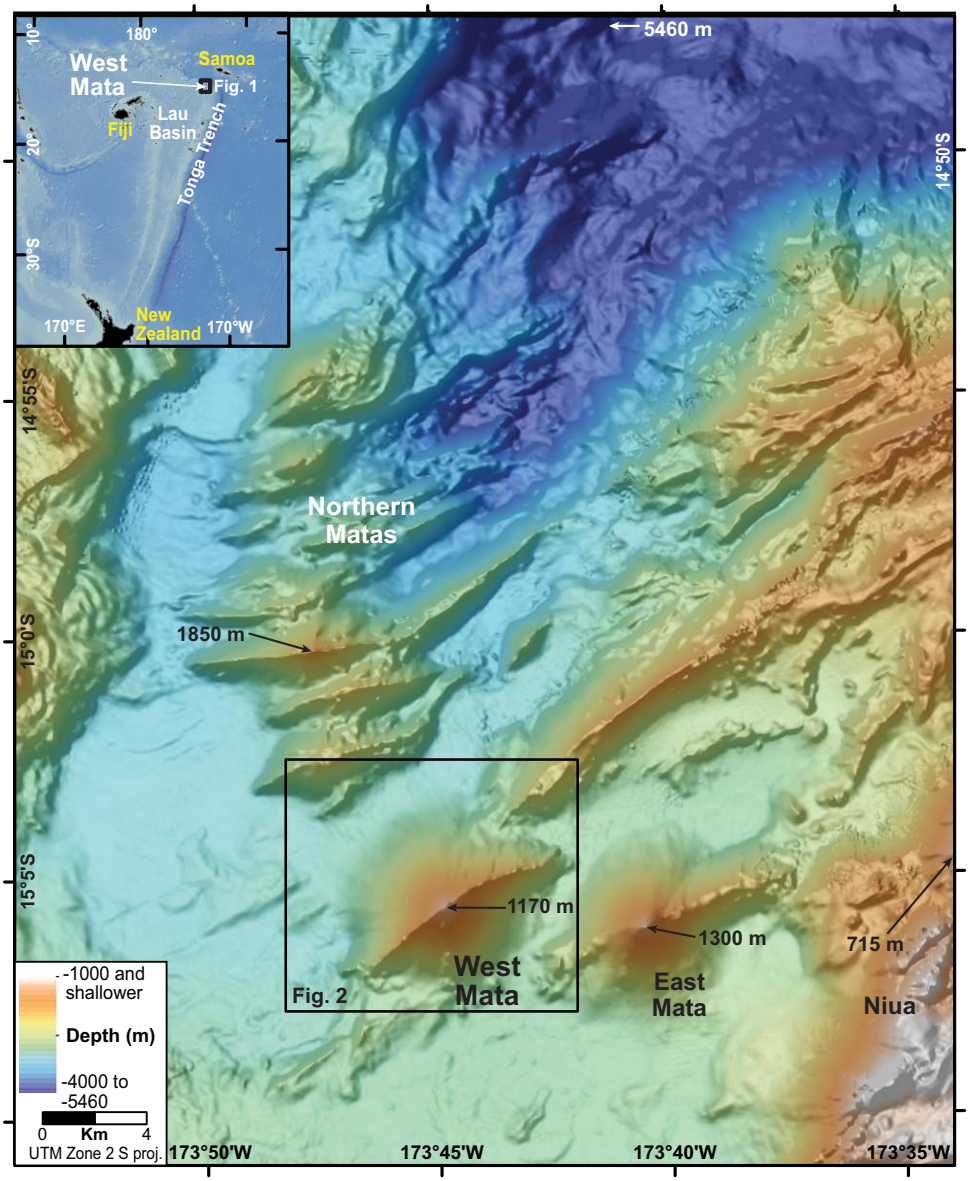

Figure 1. Regional map of NE Lau basin in the vicinity of West Mata. Inset shows location relative to Tonga Trench, New Zealand, and several islands. Also shown are selected other place names, summit depths of several seamounts, and inner wall of Tonga Trench (to the north of study region). Box shows location of Figure 2.

observations of active submarine volcanic activity have been made at just two sites, both within a magmatic arc/back-arc setting. The eruption of NW Rota-1, a seamount located in the southern Mariana arc, was discovered in 2003 [*Embley et al.*, 2006] and was still active during the last in situ observations in 2010 [*Chadwick et al.*, 2008b, 2012b]. The eruption of West Mata seamount, a submarine volcano located in the NE Lau basin (Figure 1), was detected in 2008 with water column sensors [*Resing et al.*, 2011]. Five months after the discovery of the ongoing eruption, West Mata (as it is henceforth referred to in this paper) was visited on five dives with the *Jason* remotely operated vehicle (ROV) in May 2009 when it exhibited spectacular explosive magma bursts driven by intense degassing and pillow lavas flowing downslope from two vents (Figure 2, inset) [*Resing et al.*, 2011]. Although the West Mata eruptions occurred at 1165–1205 m water depth, the high water content of the boninitic magma (possibly coupled with a higher mass eruption rate) generated a more (visually) explosive style than the much shallower NW Rota-1 eruptions at 550 m (at least during the brief seafloor observation periods) [*Resing et al.*, 2011].

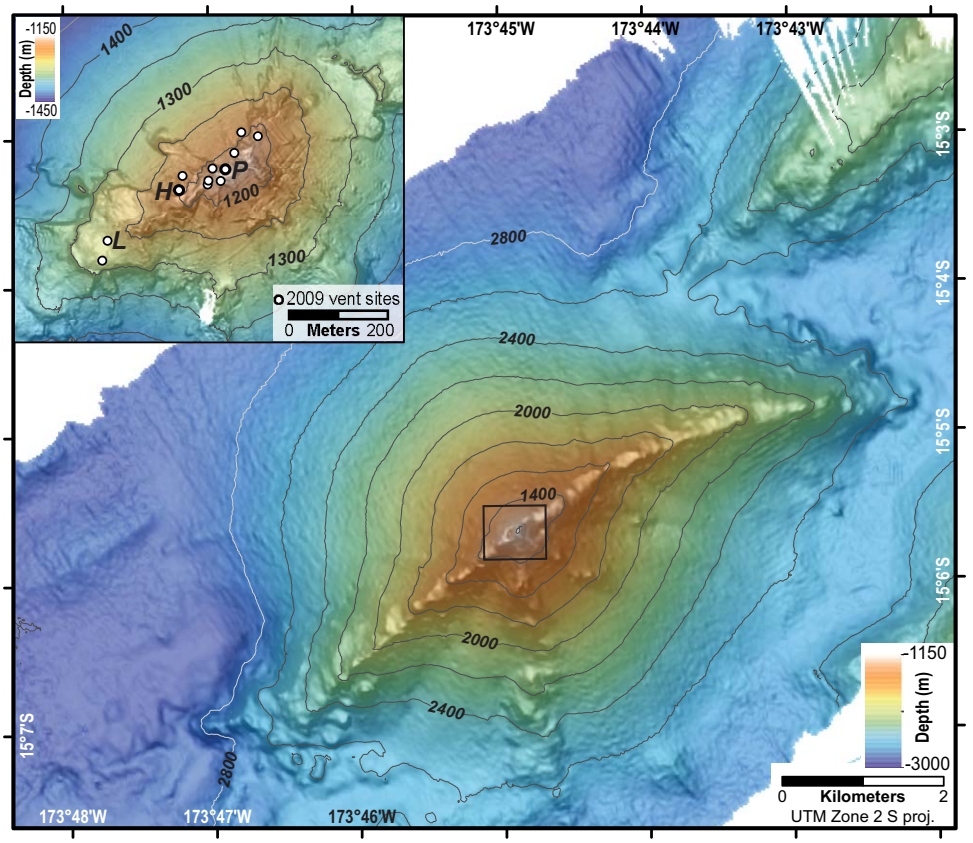

Figure 2. Bathymetry of West Mata (20 m grid cell size) from data collected in 2011 using the EM122 multibeam system on the R/V *Kilo Moana*. The contour interval is 200 m. (top left) Box at the summit shows area of inset with locations of hydrothermal and volcanic vents (white circles). Underlying bathymetry by multibeam sonar on the MBARI *D. Allan B*. AUV [*Clague et al*., 2011] gridded at 2 m grid cell size with contours at 50 m interval. Abbreviations of sites referred to in text are "H" (Hades), "P" (Prometheus), and "L" (Luo).

West Mata is located in the NE Lau basin, approximately 140 km south of Samoa (Figures 1 and 2). It and its morphologic "twin," the shallower (∼1300 m) East Mata seamount, are similar in shape and size (∼8 × 10 km), and both have been constructed with WSW-ENE/E elongated rift zones. Together with seven smaller and deeper volcanoes to the northwest, they form a modern, possibly unique, submarine boninitic volcanic province between the magmatic arc line (the northernmost extent of which is represented by Niua seamount in Figure 1) and the northeast Lau spreading center ∼40 km to the west [*Falloon et al*., 2007; *Resing et al*., 2011; *Rubin and Embley*, 2012]. The general WSW-ENE orientation of these volcanoes implies some structural control, probably induced from their location above the crustal tear/step fault where the northern Tongan subduction zone is transitioning to strike-slip motion [*Millen and Hamburger*, 1998; *Govers and Wortel*, 2005]. *Clague et al*. [2011] observed that much of the flank of West Mata consists of smooth slopes of volcaniclastic deposits, whereas lava flows occur mostly on the rift zones and lowermost flank. They also concluded that West Mata's recent volcanic activity has been restricted to the summit region.

This paper presents diverse data sets to document the complex processes occurring within a period of deepwater volcanism within a subduction zone. Continuity of active summit volcanism at West Mata during the November 2008 to early 2011 interval is known indirectly by water column observations during several visits between November 2008 and December 2010, by visual observations of explosive summit volcanic activity in 2009 and by hydrophone recordings throughout most of the period [*Dziak et al*., 2009, 2010; *Resing et al*., 2011; *Bohnenstiehl et al*., 2013a] (Figures 3 and 4). Here we also present a new analysis of bathymetric difference grids made between seven successive multibeam sonar surveys from 1996 to 2012) (Figure 3 and Tables 1 and 2). This analysis reveals significant morphologic changes, including, previously unknown eruptions of the flanks and WSW rift zone (WSWRZ), the formation of a 100 m (diameter) crater at the summit, and a landslide on the volcano's eastern flank. We also present new in situ observations made on two ROV dives in September 2012 and a time series of water column

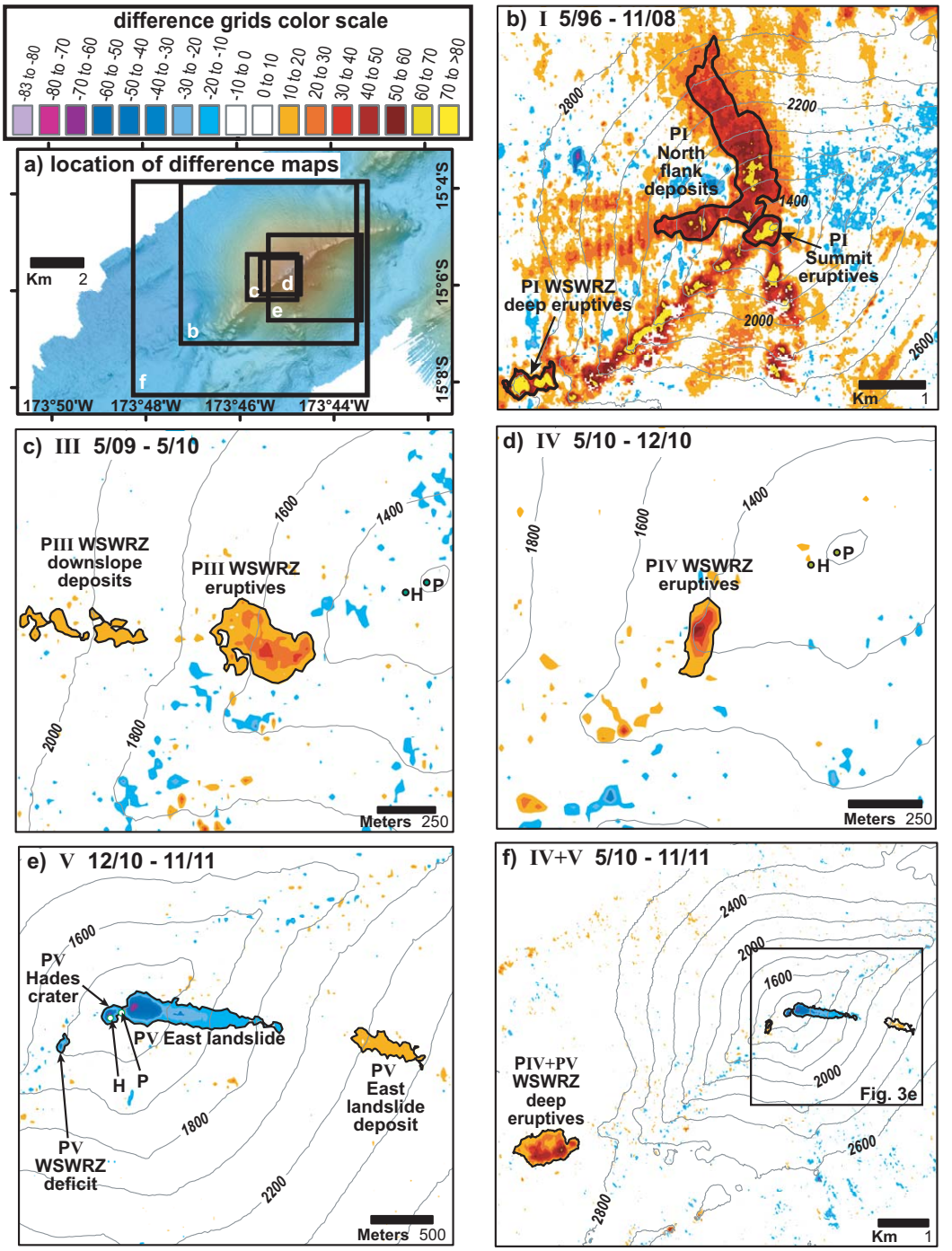

Figure 3. Multibeam difference maps for periods showing significant depth change at West Mata (see also Tables 1 and 2, supporting information Table S1 and Figures S1–S3). There were no depth changes resolvable with this technique for periods II and VI, so they are not shown here. Contour interval is 200 m for all maps. Scale and area of maps are optimized to show detail for areas of depth changes. Details of depth changes in summit area and on upper WSWRZ are shown in Figure 5 and details of depth changes on and near the southeastern WSWRZ are shown in Figure 6. (a) Area of maps in Figures 3b–3f. (b) May 1996 to November 2008 (period I). Black outlines on this and following maps on this figure indicate areas interpreted as real geologic change (see text for details). (c) May 2009 to May 2010 (period III). (d) May 2010 to December 2010 (period IV). (e) December 2010 to November 2011 (period V). (f) Difference map for expanded bathymetry grids available for May 2010 and November 2011 surveys (periods IV + V). The map shows an eruption on the extension of the WSWRZ in 2900+ m water depth (PIV + PV WSWRZ deep eruptives). Also shown are changes that occurred in period V near the summit.

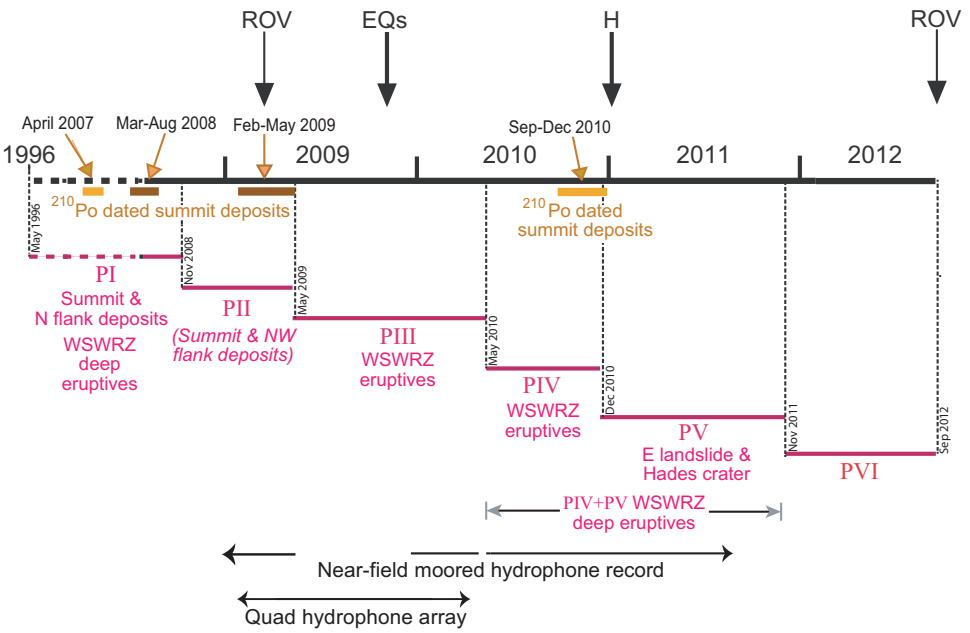

Figure 4. Timeline of six periods bounded by seven multibeam surveys (dashed vertical black lines) and other time series data and events (vertical arrows at top) at West Mata—1996–2012. Water column data were collected on all cruises except for initial survey in 1996. Note that, because of scaling needed to show details of recent history of West Mata, most of period I (12 years long) is represented by dashed line (there were no other data collected at West Mata during this period). Eruptions discussed in text (and in Figure 3 and Tables 1 and 2) appear in red below the period name. The PII summit and NW flank deposits (italicized and in parentheses) are only know from a ^{210}Po-^{210}Pb date from that period (Figure 9a and Table 3), i.e., no well-defined depth change anomaly fell outside the ±10 m depth change error bar. Period boundaries are offset to improve clarity. Thick solid brown bars below the timeline represent the cumulative age range (plus error bars) of eruption ages of lava samples collected during ROV dives in May 2009 and September 2012 (see Table 3 and supporting information Text S3 and Table S4). The two solid tan bars are for samples (one on each ROV dive series) with higher uncertainties (because they were erupted 2 years before they were collected). All of the other samples (seven of them) fit into the two brown bars of higher-resolution age data. Vertical arrows at top indicate specific events: "EQs" refers to the M = 8.1 and associated events on 29 September 2009; "H" is the approximate time of the last volcanic signal recorded by the moored hydrophone; "ROV" marks periods of seafloor visits using remotely operated vehicles. Approximate time range covered by the moored hydrophone recordings are shown by the horizontal lines with arrows at the bottom. The upper one is for near-field hydrophone records and the lower is for the hydrophone array at 20.5°S in the Lau basin [*Bohnenstiehl et al.*, 2013a].

measurements during the 2008–2012 interval. Finally, a new hydroacoustic record (May 2010 to September 2012) from a nearby moored hydrophone [*Fox et al.*, 2001] indicates that the summit eruption ceased by early 2011.

2. Data Acquisition and Processing

2.1. Multibeam Data

Bathymetric data used to calculate depth differences at West Mata were collected on seven expeditions over a 16 year period (Table 1 and supporting information Table S1) between 1996 and 2012 (Tables 1 and 2). The initial 1996 survey of West Mata utilized a SeaBeam 2000 multibeam system onboard the R/V *Melville*.

Table 1. Multibeam Sonar Surveys Utilized for Bathymetric Differencing at West Mata and Characteristics of the Sonar Systems

Month-Year	Vessel	Cruise ID	Chief Scientist	Sonar System	Frequency (kHz)	Beam Width (°)	Max Beams/Ping	Average Speed (kts)	Theoretical Vertical Error (%)	Error at 1200 m	Error at 3000 m
Jun-1996	R/V *Melville*	BMRG08-MV	S. Bloomer	SeaBeam 2000	12	2 × 2	121	10.3	0.5	6	15
Nov-2008	R/V *Thompson*	TN227	J. Lupton	EM300	30	1 × 1	135	9.5	0.2	2.4	6
May-2009	R/V *Thompson*	TN234	J. Resing and R. Embley	EM300	30	1 × 1	135	9.2	0.2	2.4	6
May-2010	R/V *Kilo Moana*	KM1008	J. Resing	EM122	12	1 × 2	288	8.5	0.2	2.4	6
Dec-2010	R/V *Kilo Moana*	KM1024	K. Rubin and R. Embley	EM122	12	1 × 2	288	5.6	0.2	2.4	6
Nov-2011	R/V *Kilo Moana*	KM1129a	F. Martinez	EM122	12	1 × 2	288	4.5	0.2	2.4	6
Sep-2012	R/V *Revelle*	RR1211	J. Resing and R. Embley	EM122	12	1 × 2	288	6.2	0.2	2.4	6

Table 2. Eruptions at West Mata From 1996 to 2012 Depth Changes, Surface Area, and Volume Calculations

Month/Year	Period[a]	Cruise ID	Depth Changes	Surface Area (m^2)	Volume (m^3)[c]
Depth Changes Between 1996 and 2008 Must be ≥ 30 m to be Included in Surface Area/Volume Calculations					
6/1996	[b]	BMRG08-MV			
11/2008	I	TN227	(1) Summit eruptives	(1) 1.8×10^5	(1) 9.6×10^6
			(2) Flank deposits	(2) 1.8×10^6	(2) 7.6×10^7
			(3) PI WSWRZ deep eruptives	(3) 2.2×10^5	(3) 1.2×10^7
Depth Changes Between 2008 and 2012 Must be ≥ 10 m to be Included in Surface Area/Volume Calculations					
5/2009	II	TN234	None within confidence range	n/a	n/a
5/2010	III	KM1008	(1) PIII WSWRZ eruptives	(1) 8.8×10^4	(1) 1.6×10^6
			(2) WSWRZ downslope deposits	(2) 3.2×10^4	(2) 3.5×10^5
12/2010	IV	KM1024	PIV WSWRZ eruptives	2.5×10^4	5.1×10^5
11/2011	V	KM1129a	(1) Hades crater deficit	(1) Neg 1.8×10^4	
			(2) East landslide deficit	(2) Neg 1.8×10^5	
			(3) East landslide deposits	(3) 7.0×10^4	(3) 8.4×10^5
			(4) PV WSWRZ deficit	(4) Neg 8.3×10^3	(4) Neg 1.4×10^5
	1V + V	KM1008 thru KM1129a	PIV + V WSWRZ deep eruptives[d]	6.1×10^5	1.6×10^7
9/2012	VI	RR1211	None within confidence range. Noisy data	n/a	n/a

[a]Period extends from previous survey date to current one.
[b]This is the earliest multibeam survey of West Mata.
[c]Volume values are positive unless noted (Neg = negative values).
[d]This event occurred between May 2010 and November 2011. No survey of base of West Mata on KM1024 (December 2010).

Those were the only data available until a series of six bathymetric surveys were conducted in the area from 2008 to 2012 with the newer Kongsberg-Maritime EM300 and EM122 multibeam systems onboard the R/V *Thompson*, R/V *Kilo Moana*, and R/V *Roger Revelle* (Table 1). Initial results of differencing the 1996 to May 2010 surveys were presented in *Clague et al*. [2011]. We have recalculated and reinterpreted those data and also present the December 2010 to September 2012 difference grids for the first time in this paper. The details of the various surveys, including track lines, survey speeds, data densities, bathymetric slopes, data processing steps, and other information are presented in Tables 1 and 2 and supporting information Text S2, Table S1, and Figures S1–S3. The acquisition, navigation, and processing of the high-resolution bathymetry collected by the Monterey Bay Aquarium Research Institute's (MBARI) *D. Allan B*. autonomous underwater vehicle (AUV) used is this paper are described in *Clague et al*. [2011].

Sound velocity profiles (SVP) were applied to the bathymetry data upon collection, with the exception of the 1996 survey. The bathymetry data from each survey were cleaned and processed using MB-System software and bathymetric grids were created at 25 m grid cell intervals with a spline-interpolated search radius of 5 times that distance. It was determined that the 25 m grid cell was the minimal size below which overgridding produced artifacts in some of the survey data. Each survey was differenced with the previous one to produce a depth change grid using the GMT (Generic Mapping Tools) grdmath command. The bathymetric and depth difference grids were brought into ArcGIS and Fledermaus software for further analysis. Surface area and volumetric calculations were constrained by polygons around areas of positive or negative anomalies, resulting in volume measurements of particular events in a focused area. A positive depth change results in a shallower depth, and a negative depth change results in a deeper depth. Those polygon constraints were chosen in areas where depth changes are geologically reasonable, e.g., small but broad positive areas downslope from eruptive vents or landslides.

The data quality of the 1996 SeaBeam 2000 survey is poorer than that of the 2008–2012 surveys because of sparser soundings and overall higher system noise [*Clague et al*., 2011]. Attempts at applying a SVP to the 1996 survey to improve the data were not successful. As determined by *Clague et al*. [2011], we applied a +10 m correction to the 1996 bathymetric grid (making it shallower). The surface area and volume calculations for the 1996–2008 period I (Table 2) presented here (i.e., comparing the 1996 to the 2008 surveys) utilize only depth changes greater than 30 m due to the lower quality of the 1996 data [*Clague et al*., 2011]. The bathymetric data collected on surveys between 2008 and 2012 have less noise and denser soundings (supporting information Figures S2 and S3). The 2008 and 2009 surveys were conducted on the R/V *Thompson* using a Simrad EM300 system; the 2010 and 2011 surveys on the R/V *Kilo Moana* (Table 1) with a Simrad EM122 system and the 2012 survey was on the R/V *Melville* with a Simrad EM122 system (Table 1). We conclude that depth differences of 10 m and greater are credible (for periods II-VI) and are used in the surface area and volume calculations presented in Table 2 (as defined in Table 2 and in section 3.1).

2.2. Water Column (NTU, ORP, Helium Isotopes, and Hydrogen)

Our main water column tool was a Sea Bird 911plus Conductivity-Temperature-Depth-Optical (CTDO) and rosette package. The CTDO package was deployed either in vertical profile mode (cast) or in "tow-yo" mode, whereby it was towed at slow speeds and concomitantly winched up and down over several hundred meter depth range in a sawtooth pattern. The package included real-time light backscattering and oxidation-reduction potential (ORP, sometimes referred to as Eh) sensors (data used in this study are in supporting information Table S2). The voltage output of the light-backscattering sensors is equivalent to nephelometric turbidity units (NTU) [*American Public Health Association*, 2007]; ΔNTU is the value relative to ambient nonplume water. The ORP (oxidation-reduction potential) sensor measures the electrode potential (*E* (mV)) between a platinum electrode exposed to seawater and a reference Ag/AgCl electrode. Because *E* declines when it encounters reduced substances, the anomalies are negative. ORP is very sensitive to short-lived reduced chemicals in hydrothermal plumes, such as Fe^{+2}, Mn^{+2}, H_2, and sulfides [*Walker et al*., 2007].

Submarine hydrothermal fluids are characterized by $^3He/^4He$ ratios that are elevated compared to air due to the presence of ^3He-rich helium in the earth's mantle. Because helium is a conservative species unaffected by any chemical or biological processes, the presence of elevated $^3He/^4He$ in the ocean is an unambiguous indicator of magmatic input. Because the changes in $^3He/^4He$ in the ocean are generally small, the ratio is usually expressed as $\delta(^3He)\%$, which is the percentage deviation of $^3He/^4He$ from the atmospheric ratio. Water samples for helium analysis were sealed into copper tubing at sea using a high-pressure hydraulic press [*Young and Lupton*, 1983] and analyzed on a mass spectrometer specially designed for helium isotope analyses (see *Lupton* [1990] for a description of methods). Hydrogen (H_2) and other gases were measured by gas chromatograph on board immediately following the sample recovery. Details of sampling and analytical methods plus additional plume chemistry, including total dissolved iron (TDFe), are in T. Baumberger et al. (Understanding a volcanic eruption through time series hydrothermal plume sampling of dissolved gases: West mata Volcano, 2008–2012, submitted to *Geochemistry, Geophysics, Geosystems*, 2014). Sampling and analysis for additional plume chemistry was conducted as described by *Resing et al*. [2009]. Details about the hydrogen and helium samples reported in this paper are in supporting information Table S3.

2.3. Remotely Operated Vehicle Navigation

ROV dives at West Mata in May 2009 and September 2012 provide some visual ground truth for the bathymetric changes. Navigation for the 2009 *Jason* ROV was by an ultrashort baseline (USBL) system, Doppler sonar for speed over bottom and a laser ring gyro for heading. The data were logged at 1 s intervals and integrated using software developed at Woods Hole Oceanographic Institution (WHOI). *Quest 4000* ROV navigation in 2012 utilized a Ashtead Technology IXSEA GAPS USBL navigation system with software modified from the WHOI ROV *Jason* group for data logging. *Quest 4000* ROV navigation data were logged at 2 s intervals when fixes were obtainable. Raw navigation files were postprocessed using smoothing algorithms available through ArcGIS software. Final navigation sometimes required visual fitting with the available high-resolution bathymetry. Both the precision and accuracy of the ROV navigation for 2009 and 2012) were within about 25 m, one grid cell on the bathymetric differencing grid. Comparison of depths between multibeam sonars and ROV pressure depths agreed within ~10–15 m over areas of smooth topography (versus steep areas where small navigation errors could result in larger apparent depth changes).

2.4. ^{210}Po-^{210}Pb Dating of Lavas

Eruption ages were determined on 10 rock samples collected from both vent-proximal and vent-distal sites on the West Mata summit (Figure 9). Most of the samples were collected on the May 2009 NE Lau response cruise (TN234). One sample from the RR1211 (2012) expedition was also dated because this young flow sample appeared to overlie a failure surface of older rock (see Table 3 and supporting information Text S3, Table S4 for list of samples and details of analysis and age dating results). Although the ^{210}Po-^{210}Pb method has been applied multiple times to young submarine lavas (summarized in *Baker et al*. [2012, Table 1]), West Mata and the 2005–2006 eruption at 9°50′N on the East Pacific Rise [*Rubin et al*., 2008, 2012] are the only instances where a large number of samples (>6) have been dated from one eruption sequence, significantly improving the spatial and temporal resolution of eruption reconstructions using eruption ages. ^{210}Po activity was analyzed in three or four ^{209}Po-spiked aliquots of dissolved fresh volcanic glass per sample over several 138.4 day half-lives [*Rubin et al*., 1994] using high-resolution isotope dilution alpha spectroscopic

Table 3. ^{210}Po Eruption Ages of West Mata Lavas[a]

Sample	IGSN	Collection Date	Expedition	S °Latitude	W °Longitude	Eruption Age	Age Error (Days)	R^2	^{210}Pb
J2–413-R02	KHR000002	6 May 2009	TN234	15.09457	173.74952	21 Mar 2009	3	0.99	0.521
J2–413-R13	KHR000008	6 May 2009	TN234	15.09430	173.74837	24 Apr 2009	1	1.00	0.523
J2–414-R12	KHR00000B	7 May 2009	TN234	15.09406	173.74806	6 Mar 2009	2	0.99	0.498
J2–414-R27	KHR00000E	7 May 2009	TN234	15.09449	173.74849	n/a	n/a	n/a	0.451
J2–417-R09	KHR000018	10 May 2009	TN234	15.09493	173.74921	17 Sep 2008	26	0.83	0.514
J2–418-R18	KHR00001I	11 May 2009	TN234	15.09468	173.74918	16 Apr 2009	2	1.00	0.520
J2–420-R16	KHR000020	12 May 2009	TN234	15.095	173.749943	25 Apr 2007	67	0.80	0.461
J2–420-R17	KHR000021	12 May 2009	TN234	15.09492	173.74904	23 Mar 2008	24	0.74	0.457
J2–420-R23	KHR000022	12 May 2009	TN234	15.09442	173.74891	12 May 2009	0	1.00	0.503
Q332-R05	KHR000109	24 Sep 2012	RR1211	15.09396	173.74778	6 Dec 2010	36	0.84	0.511

[a]Lava sample names, collection particulars, eruption ages, and ages quality assessment parameters. Eruption ages are maximum ages corrected for 9% Po retention upon eruption (equivalent to 15 days), as described in the text. Age error is the propagated error from three individual error sources (^{210}Po analysis errors—see supporting information Table S4, ingrowth curve regression errors—see also the R^2 value in the table above, and a correction for time between sample collection and first ^{210}Po analysis). ^{210}Pb is determined from the ingrowth curve regression. IGSN are international geosample numbers, registered through www.geosamples.org. ^{210}Po and age data are available at doi:10.1594/IEDA/100444.

methods on a 12-detector Canberra Alpha Analyst (supporting information Text S3). The results of 32 ^{210}Po analyses on 10 lava samples are in Table 3. Supporting information Table S4 lists ^{210}Po change with time in each lava specimen analyzed, which tracks the ingrowth of eruption-degassed ^{210}Po relative to essentially undegassed ^{210}Pb. Eruption ages were determined by exponential regression of ^{210}Po activities in aliquots of each sample. Maximum eruption ages are determined from the intercept of this curve (i.e., the calculated time since complete Po loss). Ages presented here have been corrected for a small amount of incomplete Po degassing, using the Po value found in a molten West Mata lava sample collected in 2009: sample J2–420-Rock-23 had roughly 9% of its final Po value on the day of sample collection. This small amount of retained Po equates to 15 days of ingrowth from a hypothetical initial value of zero. This value is incorporated into the eruption age errors, along with analytical error and regression errors.

2.5. Moored Hydrophone

A moored hydrophone was deployed ~5 km south of the summit of West Mata (15°07′S; 173°44′W) at 1000 m water depth (within the ocean sound channel) in May 2010 and recovered in September 2012. The hydrophone data were logged continuously from May 2010 to August 2011. The details about the instrumentation, mooring setup, and data processing are in *Fox et al.* [2001].

3. West Mata Multibeam Bathymetry Time Series 1996–2012

The use of multibeam bathymetric data to detect changes on the seafloor to analyze submarine volcanic processes began in the 1980s when an eruption on the southern Juan de Fuca Ridge was documented from comparing pre and posteruptive surveys [*Chadwick et al.*, 1991; *Fox et al.*, 1992]. Subsequent studies using this technique have documented a wide range of submarine volcanic events [*Rubin et al.*, 2012]. Of particular interest to this study is the use of the technique to analyze short-term constructional and degradational processes on arc and back-arc volcanoes [*Chadwick et al.*, 2008a; *Walker et al.*, 2008; *Wright et al.*, 2008; *Chadwick et al.*, 2012b; *Watts et al.*, 2012]. The accuracy, precision, and resolution of the technique have improved through time as newer generations of multibeam sonars with higher-resolution beam-forming arrays have come into use along with improved vessel navigation and motion sensing technology. When comparing surveys used in this study, we initially describe depth change anomalies as either positive (shallower) or negative (deeper) depth change in order to keep the observations separate from the interpretation of the geologic formation processes.

Below and in Figures 3–8 and Table 2, we summarize the changes observed during the six time periods (I–VI) defined by the seven multibeam surveys of West Mata. Figure 3 summarizes the significant depth changes of these periods and Figure 4 shows a timeline for the major events. For this study, we reanalyzed the results of the bathymetric differencing presented in *Clague et al.* [2011] and also present differencing results from later surveys (extending the timeline from 2010 to 2012). Additional information and data about the surveys and the comparisons are in supporting information Text S2, Table S1, and Figures S1–S3. Note that period I is 12 years long and uses an error bound of ±30 m (because of the lower quality 1996 data), whereas periods II–VI use an error bound of ±10 m and span a total of only ~4 years, with individual periods varying from 5 months to 1.5 years. The depth changes are cumulative for a given period, e.g., a crater formed during an early part of a period could be filled in by a later event in the same period, resulting in an opposite or zero net depth change.

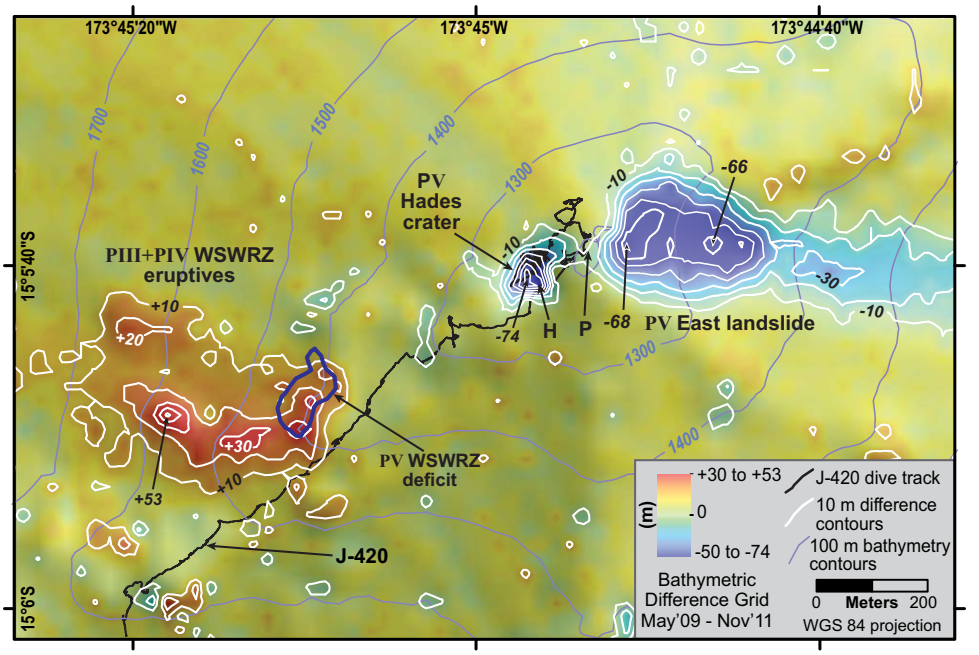

Figure 5. Details of depth change zone near the summit and upper WSWRZ of West Mata for periods III–V (May 2009 to November 2011). Points of maximum depth changes shown by arrows. "H" and "P" are Hades and Prometheus eruptive vents, respectively. Light purple lines are 100 m bathymetric contours derived from the November 2011 survey; white lines are 10 m depth difference contours. Black wiggly line is track of *Jason* dive J-420 (May 2009) along rift zone. Location of map shown in Figure 7.

3.1. Depth Changes by Survey Period

The net morphologic changes in Period 1 (between 1996 and 2008) are characterized by substantive constructional volcanism that added up to 88 m near the summit and up to 89 m on the north flank [*Clague et al.*, 2011] (Figure 3b). The ^{210}Po dating of a sample collected in 2009 indicates that summit vents were active at least as early as Spring 2007 (Table 3). *Clague et al.* [2011] also noted the occurrence of smaller

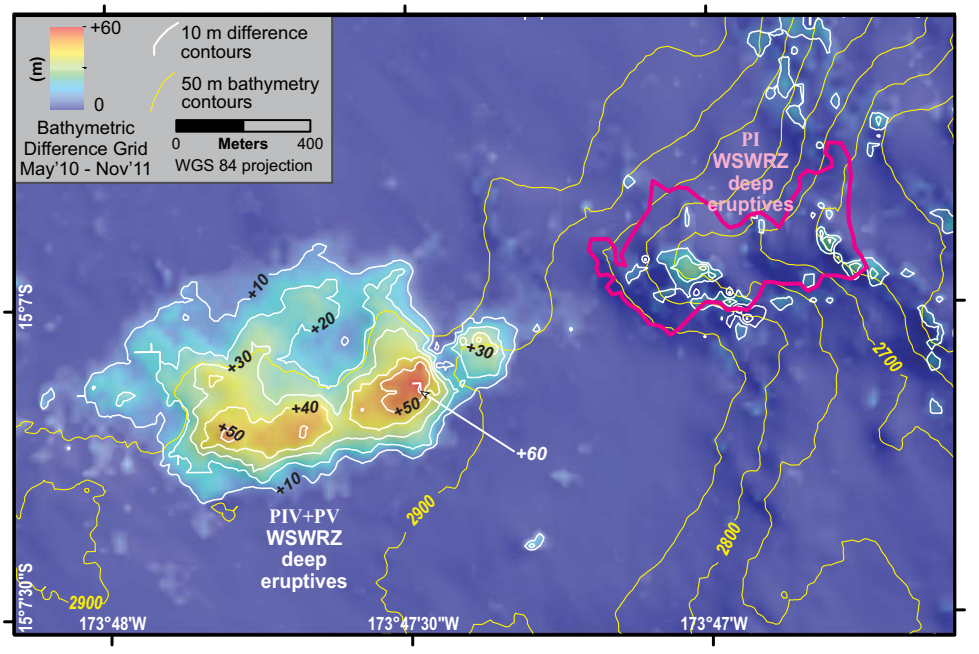

Figure 6. Details of depth change zone on and near the north extension of the deep WSWRZ for period IV + V. Yellow lines are 50 m contours derived from November 2011 survey; white contours are 10 m depth changes. Points of maximum depth changes are shown by arrows. Note also small possible positive depth change during period IV + V at ~2800 m contour within the larger outline (magenta line) of probable PI WSWRZ deep eruptives depth change zone (Figure 3b). Location of map shown in Figure 7.

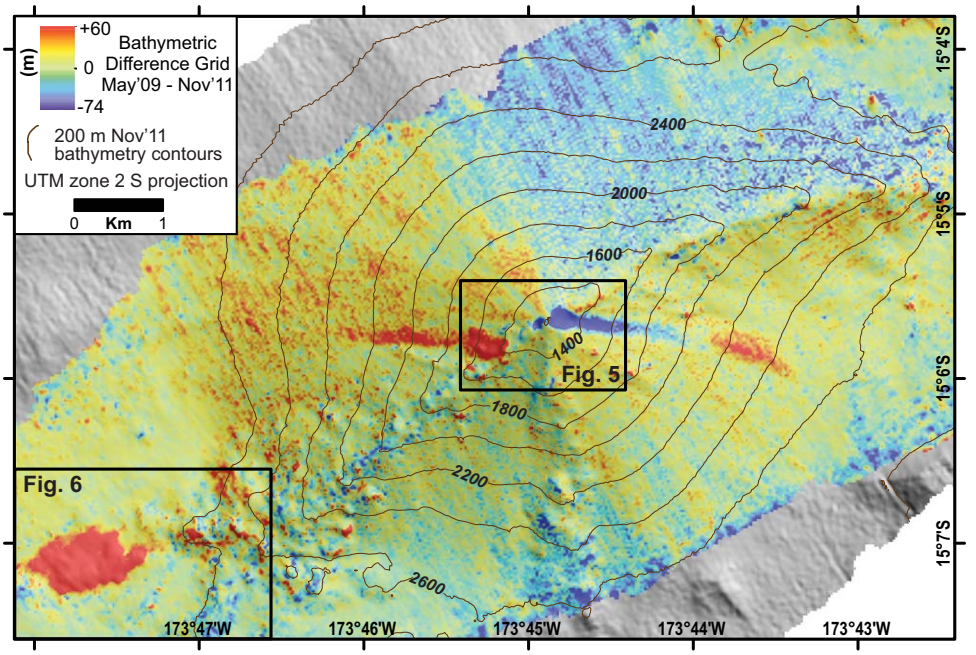

Figure 7. Depth difference grid (rainbow color scale) depicting changes from May 2009 to November 2011 (periods III–V) overlain on November 2011 bathymetric hillshade grid. Gray scale on edges is due to slightly larger 2011 bathymetry hillshade grid, although depth change grid is only calculated where the surveys overlap. Brown lines are 200 m contours derived from November 2011 survey. Location of Figures 5 and 6 shown by boxes.

positive depth changes (shoaler areas) on the WSWRZ, but did not interpret them as due to real geologic change because of the overall low data density of the 1996 survey in that area. We conclude from our reanalysis that during this period that there is one probable zone of positive depth change on the lower WSWRZ (designated as PI WSWRZ deep eruptives in Figures 3b, 4, and 6) coinciding with a region of higher data

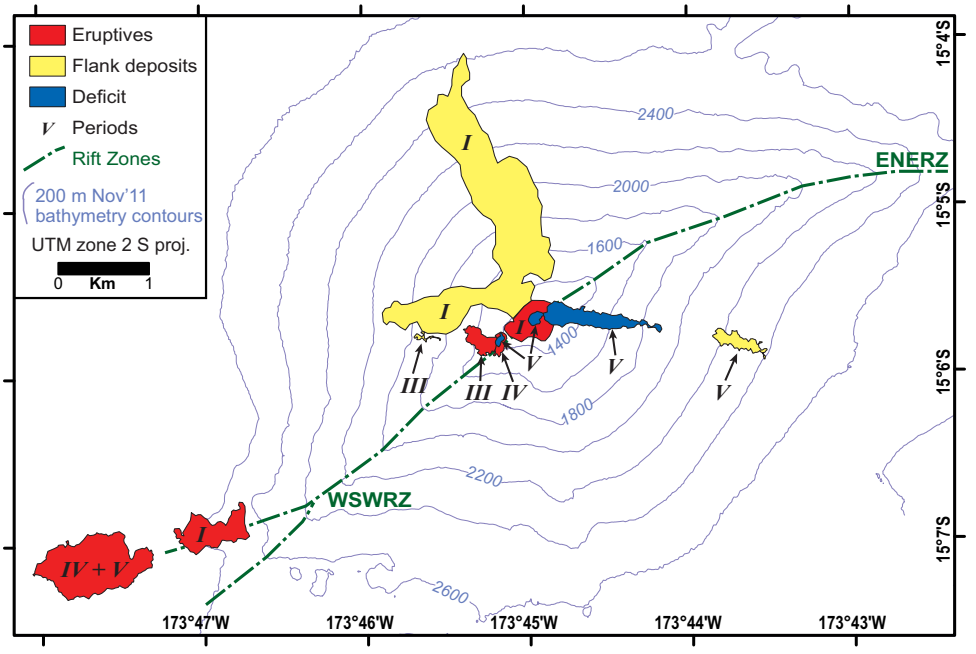

Figure 8. Summary of all depth changes from successive depth differencing of periods I–VI. Roman numerals correspond to time periods defined in Table 1. Blue contour lines same as in Figure 7. WSWRZ is the West-Southwest Rift Zone and ENERZ is the East-Northeast Rift Zone. Note that depth change zones of period I and period IV + V appear to be on or lined up with the northern bifurcation of the WSWRZ.

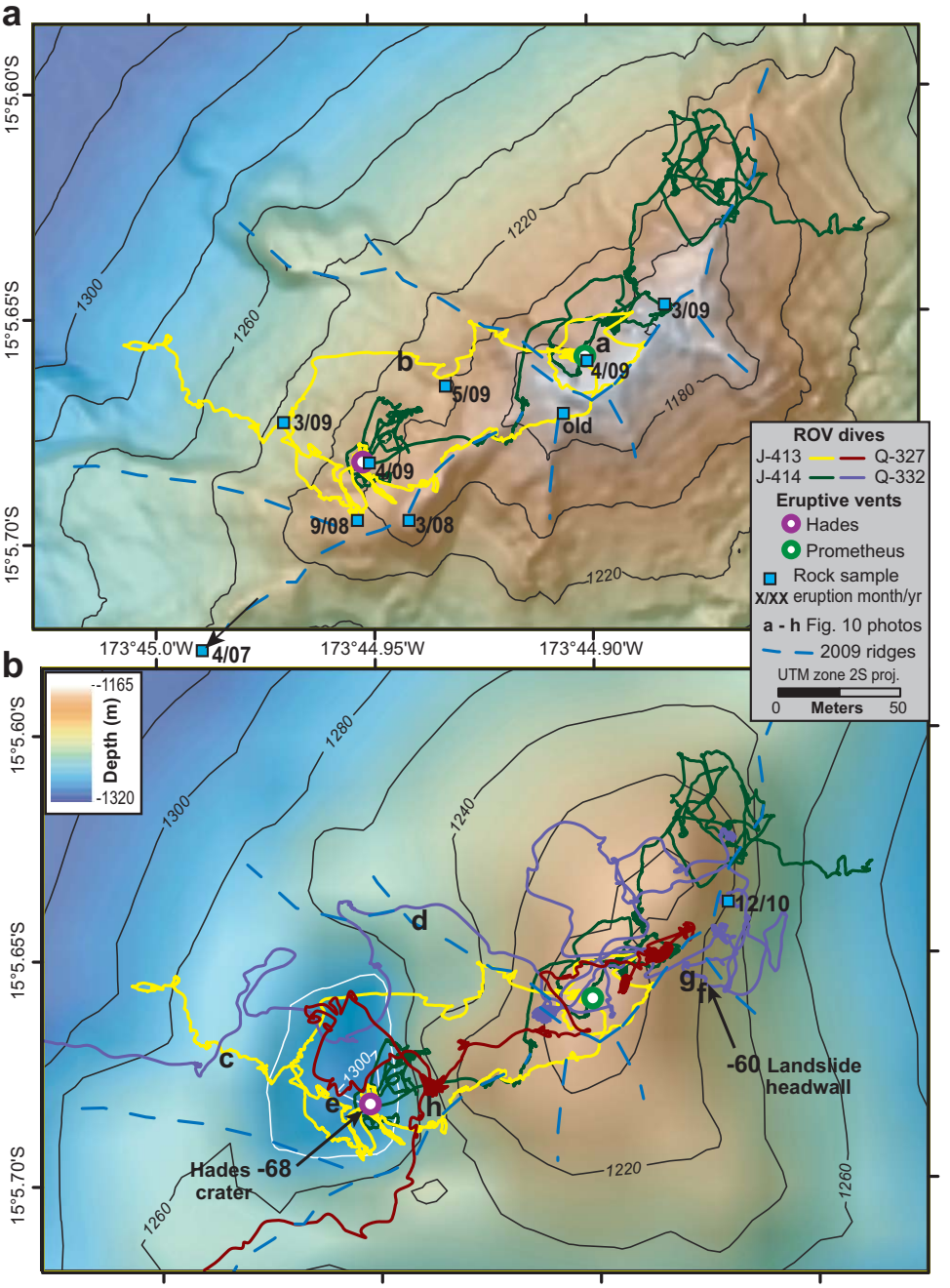

Figure 9. Summit of West Mata in (a) 2009 and (b) 2011. Letters a–h refer to Figure 10 seafloor images. (a) High-resolution 2009 MBARI *D. Allan B.* AUV bathymetry [*Clague et al.*, 2011]; 2 m grid cell size and 20 m contours. Tracks of 2009 *Jason* dives J-413 and J-414 shown as yellow and green lines, respectively. Blue filled squares are locations of samples dated by ^{210}Po-^{210}Pb method with month/year below the symbols. Dashed line is the location of primary ridges near the summit in May 2009. (b) 2011 R/V *Kilo Moana* EM122 hull-mounted multibeam bathymetry; 20 m grid cell size with 20 m contours. The PV Hades crater PV East landslide headwall area are obvious by the large changes in contours and depth differences recorded by 2012 *QUEST 4000* ROV compared to 2009 *D. Allan B.* AUV bathymetry and/or *Jason* altimeter readings (numbers of −68 m for center of Hades crater and −60 m base of headwall). Same overlays as in Figure 9a with addition of 2012 *QUEST 4000* dives Q-327 and Q-332 shown as dark red and purple lines, respectively.

density on that quadrant of the 1996 grid. There were no substantive depth changes over the ENERZ during this period, even though the 1996 survey coverage was better there than on the WSWRZ.

Period II (November 2008 to May 2009) began with the first water column survey of West Mata and culminated with our first ROV observations. Although this time interval did not have any significant depth difference above the background noise (and therefore is not shown in Figure 3), we know that the summit vents

were active and producing volcaniclastic material that moved downslope to the northwest during this period from both direct observations [*Resing et al*., 2011] and ^{210}Po dating (Figure 9a and Table 3) and so it is likely that substantial additional material was added to the north flank where the thick period I deposits are located. However, extrapolation of the average period I accumulation rate of ~4 m/yr (assuming the same area of deposition) would make the net accumulation for period II below the resolution of the technique.

The yearlong period III (May 2009 to May 2010) interval has a robust positive depth change on the WSWRZ about 0.5 km from Hades vent at ~1450 m depth (Figures 3c, 4, and 5) designated as the PIII WSWRZ eruptives. This rift zone eruptive mound was probably constructed by a combination of volcaniclastic deposits and lava flows, given its thickness (up to ~36 m), small area, and seafloor observations of pillow mounds on the rift zone near this site [*Clague et al*., 2009]. A few small positive depth change areas (~+10 to 20 m) occur downslope to the west from the rift zone site (Figure 3c), marked as PIII WSWRZ downslope deposits. Given its lack of continuity with the PIII WSWRZ eruptives, this downslope band probably consists mostly of mass-wasted material from the shallower site channelized by preexisting topography. We also note the presence of two small +5 to 10 m depth change zones downslope of Hades and Prometheus vents (Figure 3c) which, although below the depth change amplitude cutoff we use here (not shown on maps), are distinctly fan shaped in plan view so probably represent accumulation of volcaniclastic products from ongoing volcanic activity at the summit during period III.

The bathymetric depth change map for the 7 month interval (May 2010 to December 2010) of period IV (Figures 3d, 4, and 5) shows a small area of positive depth change on the WSWRZ (designated as PIV WSWRZ eruptives) on the east side of the PIII WSWRZ eruptives. The occurrence of constructional volcanism in approximately the same location as in period III implies that the eruption probably extended across the two survey periods (Figure 5). The ^{210}Po dating indicates that the summit was also volcanically active during this time period, although the full extent of the activity is not known because only one of the samples collected in 2012 was dated (eruption age of December 2010, Figure 9b and Table 3).

The most recent depth changes on West Mata were detected in Period V between surveys in December 2010 and November 2011 (Figures 3e, 5, and 7 and Table 2). Several well-defined areas of negative and positive depth change occur on the summit and east flank during period V. The largest and most distinct zone (designated as PV East landslide) is the elongate zone of negative depth change trending eastward for ~1 km from the summit area, orthogonal to the regional contours, and with maximum amplitude of −68 m at the base of the headwall near the summit (Figures 3e and 5). A small area of low-amplitude positive depth change trends downslope and east for an additional kilometer (marked as PV East landslide deposit in Figures 3e, 4, 7, and 8). Although this zone has a maximum depth change of only +17 m, it encompasses a well-defined band with minimal variability within its boundary. As their names imply, we interpret these contiguous dual zones of negative (PV East landslide) and positive (PV East landslide deposit) depth change zones resulting from a submarine landslide similar to those documented at Monowai volcano [*Chadwick et al*., 2008a; *Wright et al*., 2008; *Watts et al*., 2012] and at NW Rota-1 submarine volcano [*Chadwick et al*., 2012b]. Note that the volume of the PV East landslide (Table 2) exceeds the PV East landslide deposit by a factor of ~2. We attribute this difference in volume to a broad dispersal of material from the PV East landslide that was deposited in a thin layer below the resolution of the technique.

A small but well-defined area (~100 m diameter) of negative depth change (up to 72 m) during period V encompasses the location of Hades eruptive vent (Figures 3e, 5, and 8). On the 2011 bathymetry (Figure 9b), this area is a steep-walled depression, slightly elongated in a SW-NE direction with a maximum diameter of ~100 m. We refer to this feature as PV Hades crater in the rest of this paper. We initially interpreted PV Hades crater as a collapse crater from magma withdrawal [*Embley et al*., 2012] and one of the objectives of the September 2012 expedition (see section 4.2) was to ground truth this and the PV East landslide zone with in situ exploration using an ROV. Another small negative depth change zone on the eastern edge of the PIII WSWRZ eruptives and PIV WSWRZ eruptives (Figures 3e and 5), designated as PV WSWRZ deficit is interpreted as the collapse and/or mass wasting of a portion of the eruptives accumulated during the previous period(s).

Depth differencing of the surveys of May 2010 and November 2011 (spanning periods IV + V), which encompassed larger areas than the intervening survey in December 2010, reveals a large zone (~1.2 × 0.5 km) with up to a +60 m depth change located more than 6 km down rift from the summit in a water depth of ~2900 m (Figures 3f, 4, and 6–8). This zone is referred to henceforth as PIV + PV WSWRZ deep

eruptives. This is the largest area and volume of positive depth change for the interval from 2008 to 2012 (Table 2). The eastern edge of the PIV + PV WSWRZ deep eruptives depth change zone lies about 0.5 km from the southwestern topographic expression of West Mata (Figure 8) and its line of maximum thickness (Figure 6) is aligned approximately with the northern bifurcation of the WSWRZ (Figure 8). The thickness and shape of this depth change suggests that it represents a large lava flow. This would be consistent with the idea that compared to the summit's gas-driven fragmental eruptions, the much higher hydrostatic pressure in this deep zone should limit the extent of gas exsolution [*Head and Wilson*, 2003; *Clague et al*., 2009], and likely result in a substantially higher proportion of effusive flows relative to pyroclastics [*Clague et al*., 2011].

No significant depth differences were observed in the ~8.5 month long period VI (November 2011 to September 2012). As discussed below, this result is consistent with other evidence indicating an end to the eruption by early 2011.

3.2. Summary of Constructional and Degradational Events

Repeated bathymetric surveys at West Mata document multiple eruptive vents at varying locations and with different eruptive styles between 1996 and 2012. During the long 1996–2008 time period, there was significant volcanic construction at the summit and on the north and west flanks. We also document a (probable) eruption deep on the WSWRZ at ~2600 m. During the 2008–2011 interval (PII-PV), differencing of successive surveys documents several eruptive events on the WSWRZ and near the SW base of the volcano, culminating with a cratering event and flank failure at the summit. There were no significant depth changes resolvable by this technique on the ENERZ during the entire 1996–2012 interval.

The seafloor observations made at West Mata in 2009 [*Resing et al*., 2011], along with geologic inferences made from other studies of submarine and subaerial volcanoes, allow us to interpret the origin of the depth change zones. Eruptions can be effusive, producing lava flows, explosive, producing fragmental material, generated by magmatic gas exsolution (pyroclastic), or interaction with seawater (hydroclastic). *Resing et al*. [2011] showed that both effusive and pyroclastic material were being produced simultaneously during the summit eruptions at West Mata, i.e., the explosive degassing events also were producing degassed pillow lava flows. The relative importance of contact seawater explosivity at this site is more difficult to determine but in any case, most of the volcaniclastics generated at the West Mata vents form an apron extending away from the summit and rift zones. Much of this apron is probably constructed in a quasi steady state mode while the eruption continues, reaching an equilibrium angle of repose of ~30–35° for sand size material on subaqueous slopes. The slopes on the upper flanks of West Mata are in this range (supporting information Figure S1) following the cessation of activity. We directly observed such slope failures during ROV dives on West Mata in 2009 and on NW Rota-1 in 2006. At least some of the large deposits of period I on the north and west flanks of West Mata [*Clague et al*., 2011] were probably formed by this mechanism. Flank deposits such as those formed during period V on the eastern flank of the volcano (PV East landslide deposits) also can be emplaced by submarine landslides triggered by magma intrusions, withdrawal or by tectonic earthquakes [*Chadwick et al*., 2012b]. The PV East landslide was presumably triggered by one of these mechanisms. As noted above, over the long term, these two modes merge together, i.e., with enough output from the source vents there would be constant loading and continuous failure of the slope. The slope of the upper flank of West Mata is at the angle of repose of ~30–35° [*Clague et al*., 2011] (supporting information Figure S1) so very little loading has to be added to trigger downslope movement. Lava flows observed during ROV dives on the rift zones and summit [*Clague et al*., 2011] were probably also significant components of the summit construction during period I and in the rift zone eruptions of periods III, IV, and V.

The (probable) P1 WSWRZ deep eruptives and the well-defined PIV + PV WSWRZ deep eruptives location at and just off the topographic base of the volcano indicates that the edifice is growing at its base as well as adding material at its summit during the 1996–2012 period. These deep events probably had a higher ratio of lavas to volcaniclastics based on their morphology.

4. Seafloor Observations

4.1. 2009 Jason ROV Dives

Jason ROV dives in May 2009 (J-413, J-414, J-417, J-418, and J-420) documented never-before-seen active volcanic processes at the summit of West Mata [*Resing et al*., 2011] where two volcanic vents were in a state

of chronic eruption during the period of ~11 days on site. The most dramatic eruptions were at Hades vent ("H" in Figure 9a), located ~45 m below the summit at 1207 m on the uppermost northwest flank of the volcano. Magmatic volatiles periodically (at seconds to minutes-long intervals) formed large bubbles that produced showers of pyroclastic material [e.g., *Resing et al*., 2011, Figure 3; *Rubin et al*., 2012, Figure 2]. Prometheus, a second eruptive vent, (Figure 9a) located ~100 m northeast of Hades near the topographic summit of West Mata (~1173 m), exhibited less dramatic but more continuous activity that produced and recycled fragmental pyroclasts (Figure 10a). In addition, the first-ever observations of active deep-sea pillow lava flows were also made as the degassing lava emerged from the vent during/following these bursts and flowed tens of meters downslope in long tubes (Figure 10b; also see additional images in *Resing et al*. [2011] and *Rubin et al*. [2012]).

In addition to the eruptive sites, diffuse hydrothermal venting with exit temperatures up to 30°C occurred at numerous sites along and close to the summit area where colonies of vent-endemic shrimp swarmed [*Resing et al*., 2011] (Figure 2, small circles on inset). The summit area was composed of young lava flows and volcaniclastic material, with evidence of recent mass wasting on the steeper flanks. The only tectonic feature observed during the dives near the summit was a ~10 m long, 1 m wide fissure on the upper WSWRZ that was venting diffuse fluids (Luo vent marked as "*L*" in inset of Figure 2).

4.2. September 2012 QUEST 4000 ROV Dives

Two dives with the *QUEST 4000* ROV were made in September 2012 at the summit of West Mata in order to ground truth the areas of depth change and compare to the observations made during the *Jason* ROV dives in 2009 (Figures 9a and 9b). Depth recorded on the pressure gauges from the *Jason* ROV in 2009 and the *QUEST 4000* agreed within ~±10 m in areas where there was no geologic change such as the Luo vent (marked "L" in Figure 2, inset). Dive Q-327 traversed southwest to northeast along the summit ridge with an excursion into the Hades crater (Figure 9b). Dive Q-332 approached the crater from downslope, surveyed the edge of Hades crater, passed over the northeast summit and traversed from east to west up the headwall of the East landslide.

4.2.1. Seafloor Observations at Hades Crater

The flank of the volcano immediately downslope of the crater observed on dive Q-332 appeared to be similar in depth and geology to that observed in 2009 on J-413 (Figures 9a and 9b), with mixed tube-like pillow flows and volcaniclastic material sloping continuously upward to Hades vent. In 2012, a well-defined and visually spectacular crater rim was encountered at the location identified in the 2011 bathymetry (Figure 9b).

The northwest rim of the crater is a series of pillow flows sheared on their upslope side and often left "hanging" in space (Figures 10c and 10d). The interior of the pit was irregular with truncated-pillow faces and other sheared volcanic layers outcropping on the steep, high-relief southeast wall (Figure 10e). The 2012 observations of the interior of Hades crater show that it is a deep, steep-walled crater with a relief (~80 m) and width (~60–100 m) that coincides with the period V multibeam depth change zone. We interpret the steep walls, the "hanging" sheared pillows and the relatively smooth outer slope to be consistent with a collapse origin rather than an explosive event as the crater-forming mechanism. An explosive crater would be expected to produce a pattern of ejecta that fines from proximal to distal locations, which was not observed on several dive transects of the area around the crater. Assuming the crater formed before the end of the hydrophone recording period (September), an explosive eruption would presumably have also generated a noise loud enough to be detected on the moored hydrophone ~3 km to the southeast but no such signal was recorded (see also section 6.2).

4.2.2. Seafloor Observations at East Landslide

Depth differences up to −60 m (compared to the 2009 *D. Allan B*. AUV and *Jason* ROV depth data) were observed by the *QUEST 4000* ROV at the base of the headwall of the PV East landslide, similar to the maximum depth change in this area from the multibeam comparison. The video observations on dive Q-332 revealed a near-vertical east-facing cliff near the position of the largest negative depth anomaly with the base of the headwall clearly defined by the intersection of a debris slope and a vertical scarp of truncated lava flows (Figure 10f). The scarp face showed a succession of volcanic strata intruded with dikes (Figure 10g) striking approximately parallel to the long axis of the volcano (~N060°E). We also observed a brecciated, inverted cone structure exposed near the upper portion of the wall that we interpret as the cross

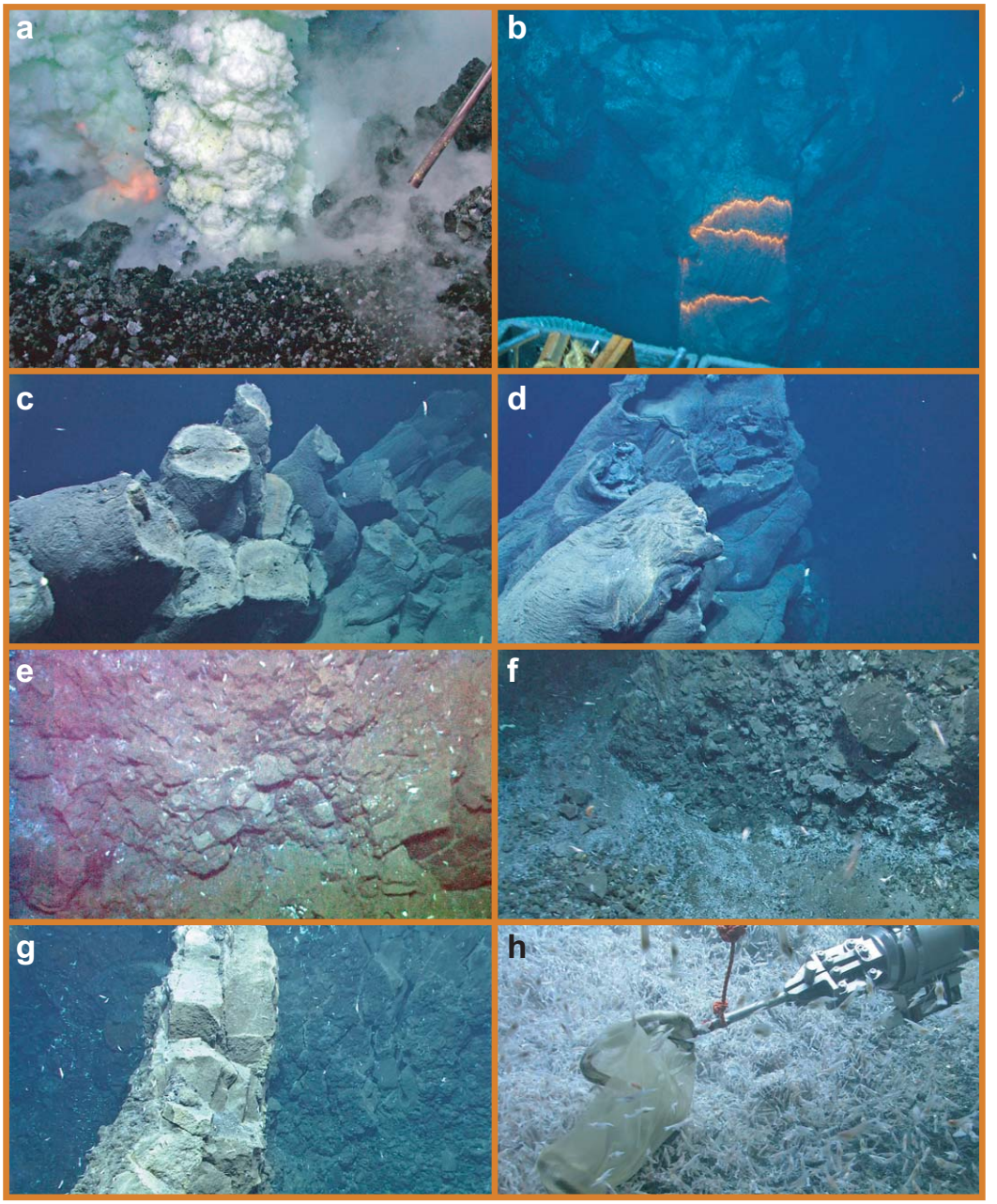

Figure 10. Images of geology and biology at West Mata in May 2009 (a and b) taken with the *Jason* ROV and September 2012 (c–h) taken with the *QUEST 4000* ROV. Locations of images are shown in Figures 9a and 9b. (a) Prometheus vent eruptive activity in May 2009. Scene is ~1.5–2.0 m across. (b) Pillow lavas flowing downslope from Hades vent in May 2009. Scene is ~3 m across. (c) Looking N-NE along the rim of Hades crater in 2012. Truncated pillows (~0.3 m diameter) hang in space on the inner slope of the crater. (d) Looking north along the rim of Hades crater in 2012 at drained-out pillow tubes (~0.4 m diameter) with hollow centers. (e) Southeast vertical wall of Hades crater in 2012 showing exposures of pillow flows and volcaniclastic units. Scene is ~3 m across. (f) Base of the headwall of the East Landslide in 2012. Scene ~3 m across. (g) Dike (~0.5 m thick at base) left intact in the headwall area of the East Landslide in 2012. (h) Sampling a shrimp swarm on the summit of West Mata in 2012. Diameter of net is ~0.5 m.

section of a collapsed volcanic vent deposit, infilled with near-vent ejecta. In 2012, only a few pinnacles of steep-outcrops and spines of lava remained of the northeast portion of the summit region.

Zones of diffuse venting on and near the summit in 2012 were colonized by shrimp swarming in much higher concentrations than observed in 2009 (Figure 10h). In addition to the population explosion of the shrimp, the vent-endemic community greatly increased in diversity from just a few species in 2009 [*Resing et al.*, 2011] to more than 10 in 2012 [reported by author T. Shank in *Resing et al.*, 2012].

5. Summit Eruption Chronology From Radiometric Lava Dating

The ^{210}Po-^{210}Pb eruption ages (Table 3) were determined on selected rock samples to map the chronology of lava flows in near-vent and vent-distal locations, to help constrain the duration of the summit eruption that was discovered in 2008, and to test aspects of the dating method. All samples are orthopyroxene + clinopyroxene + olivine phyric, highly vesicular boninite lavas, as described in *Resing et al*. [2011]. Samples were chosen for dating based on collection location, quality, and abundance of volcanic glass. A molten lava sample was collected from the base of an actively accreting pillow mound, located about 50 m north-downslope of Hades vent, to test Po retention in just-erupted lavas (see supporting information Text S3 for details). All of the other samples were solidified lava when collected.

Several observations can be made from the distribution of ages (Figure 9). Sites near the active vents and downslope to the north of the vents were mantled by lavas erupted in 2009. In contrast, lavas from the ridge south of Hades vent were erupted the year before (2008). In the past (as recently as 2007), the summit activity extended several hundred meters SSW down rift to Luo vent (Figure 2, inset). Several samples collected more than 50 m from an active vent in May 2009 were erupted in March 2009, which is the time period of the most intense acoustic signal detected by a regional moored hydrophone as described in *Resing et al*. [2011]. Taken together, the age dating and the hydrophone record imply that the summit eruption was significantly more active and that activity was occurring over a larger area about 2 months before the May 2009 expedition (TN234). One of these lavas (March 2009; Figure 9a) was collected near Shrimp City, a site that had the highest density of shrimp colonization on the West Mata summit in May 2009, perhaps providing a constraint to the time scale of ecosystem development.

The distribution of lava ages beneath or adjacent to the Hades vents implies an interesting mode of lava emplacement for pillow mounds at West Mata. Different areas appear to have erupted at different periods of time, with activity moving clockwise around the vents, implying that such pillow mounds grow in sectors. Observations made in May 2009 indicate that these mounds accrete by both surface overtopping and outflow at the base, which contributes to their expansion.

A lava sample collected in 2012 (Figure 9b), near the top of the PV East landslide headwall and northeast of the former Prometheus vent site, was dated 6 December 2010. This end date is direct (in situ) evidence that the summit eruption was active for at least 3.5 years (from Sprint 2007 to late 2010). This date is about 2 weeks prior to the start of Period V during which the PV East landslide occurred. The truncated-pillow faces observed at this site on the dive Q-332 ROV video are geologically consistent with the age dating (i.e., the pillows were sheared during the landslide), so this lava flow was one of the last eruptions before the landslide event.

6. Other Time Series Data

6.1. Water Column Anomalies

A 4 year time series of the maximum ΔNTU and ORP measured during vertical CTDO casts and tows in 2008, 2009, 2010 (April to May and December), and 2012 over the summit of West Mata (Figure 11a) shows, overall, a decrease in plume intensity and rise height with time (Figures 11b–11d). Plume anomalies and rise height were uniformly high in 2008, and generally high but variable in 2009–2010. ΔNTU, ORP, and $\delta(^3\mathrm{He})\%$ decreased in 2009, but the H_2 maximum was unchanged from 2008, indicative of an active eruptive environment continuing into 2009. Plume anomalies during the two cruises in 2010 were erratic, suggesting increasingly intermittent activity as the West Mata eruption cycle began winding down. For example, during the first 2010 cruise, we observed a robust and unusually shallow plume between 950 and 1000 m on April 29, higher than any other plume previously detected at West Mata (Figure 11b). Four days later, another profile at the summit found no evidence of this plume. The additional ~100 m rise height of the shallow plume requires a buoyancy flux ~30× higher than that estimated for the deep plume (assuming a single vent source in both cases). These observations imply a powerful but brief eruption, consistent with our acoustic observations showing that between December 2009 and April 2010 the highest daily average of sound intensity levels occurred during late April [*Resing et al*., 2011].

By December 2010, the deep ΔNTU plume was barely detectable, though ORP anomalies were present <100 m above the seafloor (Figure 11c). This combination suggests that the high-temperature eruption

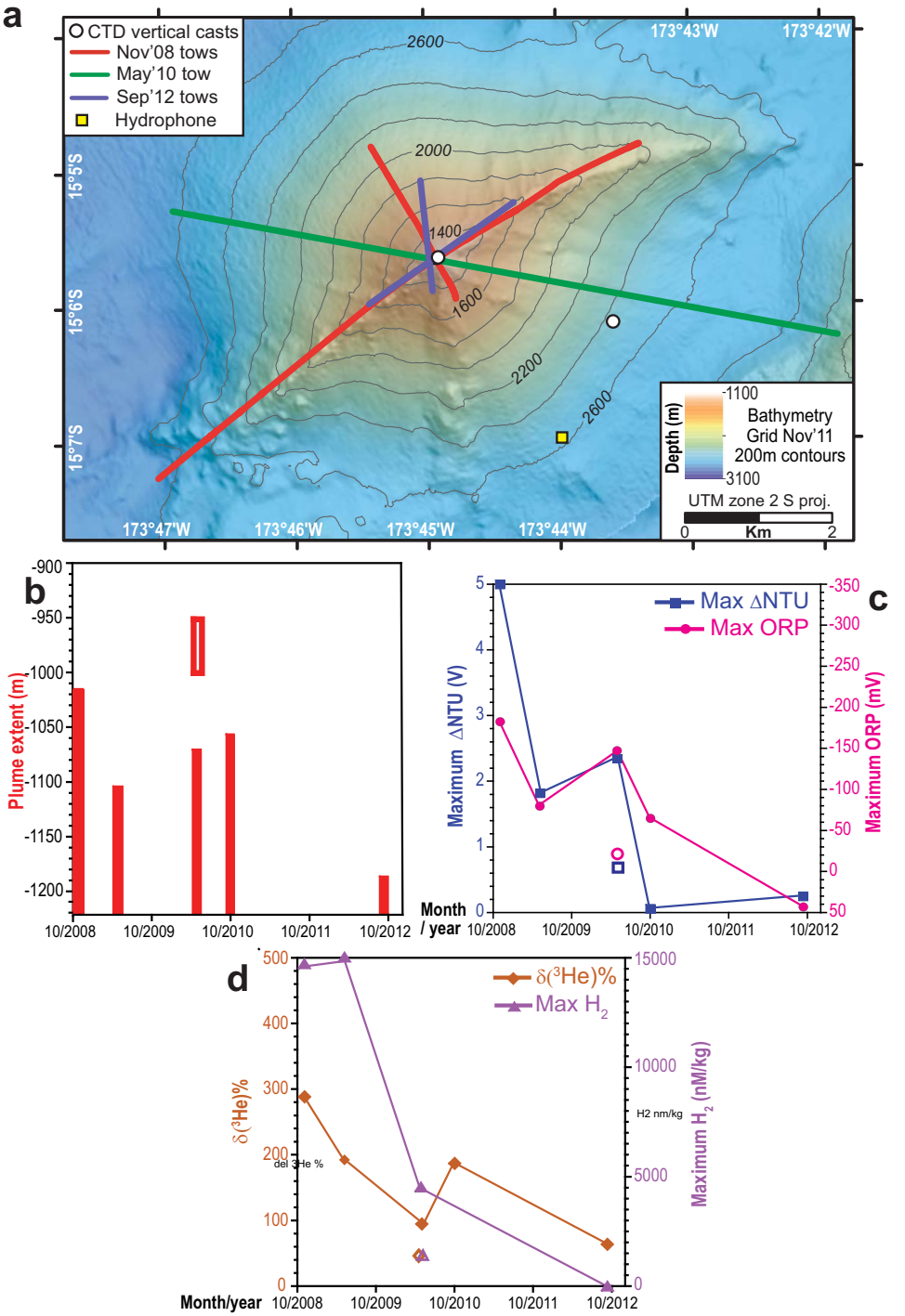

Figure 11. Summary of water column time series observations. (a) Location map showing vertical casts (white circles) and tow-yo paths (colored lines) conducted over West Mata, 2008–2012. Multiple casts at summit plot in same place at this scale. Yellow-filled square shows the deployment location of the moored hydrophone deployed from May 2010 to September 2012. (b) Thickness of the chronic near-bottom plume (solid bars) and the once-observed (April-May 2010) shallow plume (open bar) defined by ΔNTU and ORP anomalies. All plume thicknesses extended to a nominal bottom depth of 1220 m. (c) Maximum values for ORP (negative values indicate a larger anomaly) and ΔNTU in the near-bottom (solid symbols) and shallow (open symbols) plumes. (d) Maximum values for H_2 and the corresponding $\delta(^3He)\%$ values in the near-bottom (solid symbols) and shallow (open symbols) plumes. No H_2 samples were collected in December 2010. All maximum values and plume thicknesses were taken from a single cast or tow representative of each cruise with one exception. Instrument failures in 2009 necessitated using a transmissometer rather than a light-backscatter sensor on cast V09C05; those values were converted to ΔNTU. The absence of ORP data on V09C05 necessitated substituting an ORP maximum value from V09C01, also over the West Mata summit. See supporting information Text S1 (README) and Table S2 for more information and values.

venting had largely ceased, with only the lower-temperature diffuse hydrothermal venting continuing. Tows in 2012 confirmed the near cessation of venting, finding only minimal anomalies in both ΔNTU and ORP.

Elemental hydrogen (H_2) was at regional background levels in 2012 compared to a record (for submarine hydrothermal systems) high of ~15 μM in 2008 [*Resing et al.*, 2011; *Baumberger et al.*, 2014] (Figure 11d). This was a very significant change because an elevated level of elemental hydrogen is unique to magma/seawater interaction [*Sansone et al.*, 1991; *Lilley et al.*, 2003]. The temporal trend of $\delta(^3He)\%$, an unambiguous indicator of magmatic input, follows that of other tracers and confirms the magmatic control of the venting processes. Using measurements from the same water samples that contained the highest H_2 values, $\delta(^3He)\%$ declines from a high of 286% in 2008 (note that the highest $\delta(^3He)\%$ value in 2008 was ~450%, as reported by *Resing et al.* [2011] but this sample was taken from a different cast than the highest H_2 measurement) to ~55% in 2012, indicating a general decrease in hydrothermal output over this time interval (Figure 11d). In a similar fashion, total dissolvable Fe values decreased from a high of 3.3 μM in 2008 to 1.2 μM in May 2010 and to 0.17 by December 2010.

Active arc volcanoes also produce flank plumes generated by density currents of fine volcaniclastics from the summit vents. Such dense particle plumes, lacking a hydrothermal signature and containing shards of volcanic glass, have been observed around NW Rota-1 [*Embley et al.*, 2006; *Walker et al.*, 2008], Monowai [*Walker et al.*, 2010], and Kavachi [*Baker et al.*, 2002]. *Walker et al.* [2009] interpreted particle plumes present over the deep flank and adjacent western basin of West Mata in 2008 and 2009 as density flows from the summit vents. No hydrothermal plume was detected with an origin depth range consistent with either of the rift zone eruptions.

6.2. Moored Hydrophone Record

A succession of moored hydrophones, several of which were deployed ~3 km south of West Mata (location in Figure 11a), provided almost continuous hydroacoustic monitoring of West Mata from January 2009 to August 2011 (Figure 4) [*Resing et al.*, 2011; *Bohnenstiehl et al.*, 2013a, 2013b]. The hydrophones were deployed within the ocean sound channel on moorings anchored to the seafloor. The acoustic records from the moorings near West Mata and from a hydrophone array at 20.5°S in the Lau basin (recorded from January 2009 to April 2010) show that the volcano was almost continuously active from January 2009 to late 2010 [*Dziak et al.*, 2009, 2010; *Resing et al.*, 2011; *Bohnenstiehl et al.*, 2013a, 2013b; *Dziak et al.*, 2013]. Figure 12a shows a data record from the final mooring that recorded for ~1.3 years from May 2010 until the data logger stopped in September 2011. From May to October 2010, there were numerous quasiperiodic bursts of wideband explosion energy (e.g., Figure 12b). The 2010 wide-bandwidth bursts are similar to the activity recorded on the previous hydrophone data from 2009 when explosive eruptions were observed on the seafloor [*Resing et al.*, 2011]. However, there is a clear decrease in the eruptions' explosion energy at frequencies greater than 75 Hz by late September, early October of 2010. This can be also seen in the disappearance of harmonic energy present in the ~120 and ~240 Hz bands. These high-frequency tremor-like bands of energy observed at West Mata are not caused by resonance like classic volcanic tremor, but rather are a result of interference caused by the interaction of sea-surface-reflected acoustic phases with the phases that propagate directly to a nearby (<10 km) hydrophone [*Matsumoto et al.*, 2010, 2011; *Dziak et al.*, 2013]. These interference patterns are only observed when the explosion intensity is relatively high, with a large amount of acoustic energy above 50 Hz [*Dziak et al.*, 2013].

The 2010 periods of intense explosion activity gradually decreased through October, becoming much less frequent in November (Figure 12a) and had almost ceased by December 2010, with a final short burst on December 20 (Figure 12c). There were also several possible events in early 2011 [*Dziak et al.*, 2013]. There are two prolonged periods (~1 month) of high broadband energy in February 2011 and again during June to July 2011. These increases were, however, probably caused by significant regional seismicity associated with the numerous active plate boundaries in the region. A spectral analysis of the entire hydroacoustic time series did not reveal any unusual large impulsive events that could have been associated with the formation of the Hades pit crater or the East landslide [*Caplan-Auerbach et al.*, 2014]. However, these signals could have been masked or occurred after the hydrophone record ended in September 2011 (although the latter seems less likely for the Hades crater formation, which presumably formed during the last stage of volcanic activity in early 2011). Although there is a gap in moored hydrophone data from August 2011 to September 2012, a short-term (~6 h) seafloor deployment of a hydrophone within ~200 m of Hades vent on dive Q-327 in September 2012 did not record any explosive activity.

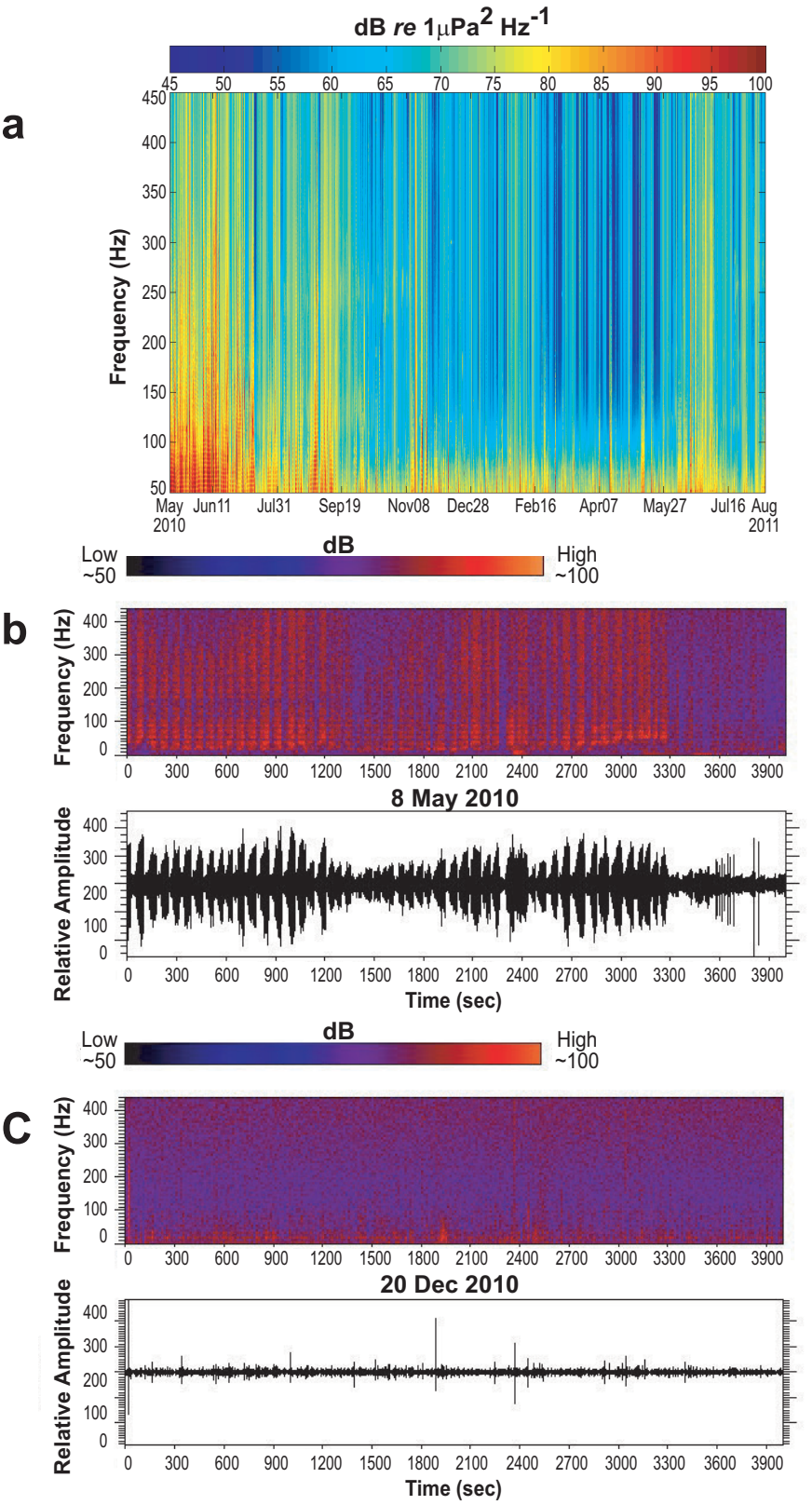

Figure 12. Hydroacoustic time series from May 2010 to September 2011 from hydrophone moored ~3 km south of the summit of West Mata (see Figure 11a). (a) Spectrogram and acoustic level (dB) of entire time period. (b) Sample spectrogram, acoustic level (dB), and relative amplitude of active period in May 2010; (c) Sample spectrogram, acoustic level (dB) and relative amplitude at end of eruptive period.

7. Discussion

Understanding of submarine volcanic activity is in its infancy. Most of the documented historical deep-sea eruptions have been short-lived effusive events on the Juan de Fuca Ridge and East Pacific Rise [*Rubin et al*., 2012]. Prior to the discovery of the long-term eruptions at NW Rota-1 and West Mata, volcanic activity within intraoceanic subduction zones had only been known from island volcanism, very shallow-water activity which manifests itself at the ocean surface, or occasionally by earthquake swarms recorded by seismometers on nearby islands or by hydrophones [*Norris and Johnson*, 1969; *Johnson*, 1973]. However, the low-level Strombolian activity at NW Rota-1 at ~520 m depth in the southern Mariana arc persisted for at least 8 years (2003–2010), mostly without any signals recorded on seismometers on nearby islands [*Chadwick et al*., 2012b]. This implies that only the shallowest (eruption depth) events and/or the most explosive events are consistently recorded by current global monitoring. West Mata, the volcano that provided us with amazing sights and insights during its active eruptive phase in 2009, is continuing to provide new information about the longer-term behavior and eruption modes of subduction zone submarine volcanoes.

7.1. Recent History of West Mata

We do not know the inception date of the eruptive activity, only that the volcano was active for some part of period I, adding material to the summit, northwest flank and probably the WSWRZ. We assume that the summit was active starting at least as early as April 2007 (based on ^{210}Po-^{210}Pb dating), more than a year prior to its discovery in November 2008. However, we do not know how continuous the activity was before the hydroacoustic time series began in January of 2009.

Sometime in period III (May 2009 to May 2010), an eruption occurred on the WSWRZ ~0.5 km southwest of Hades vent at ~1400 m depth (PIII WSWRZ eruptives). This portion of the rift zone was traversed and sampled on *Jason* J-420 (from 1570 m water depth up to the summit) in May 2009 (Figure 5), during which time there was no evidence for young or active volcanism. Rather, lava flows in this area were dusted with sediment and sparsely colonized. This suggests that the eruption in period III occurred at a site on the WSWRZ that had a significant hiatus in volcanic activity. This site was also active during some portion of period IV (May to December 2010). A large eruption (PIV + PV WSWRZ deep eruptives) occurred between May 2010 and November 2011 (periods IV + V) near the southwestern base of the northern deep branch of the WSWRZ at ~2950 m just west of the PI WSWRZ eruptives (Figures 6 and 8). None of these WSWRZ eruption sites were visited by the *QUEST 4000* ROV in 2012 because we were not aware of their existence at the time of the expedition and there was no information suggesting these sites were active. The water column time series implies that the summit activity on West Mata was gradually declining from November 2008 to December 2010, although the high-rising plumes observed in April 2010 may attest to some intense eruptions late during that period. By the end of 2010 or beginning of 2011 the volcano's summit eruptive activity had ceased and during or (probably) soon after that, a small crater formed under one of the main eruptive vents and a landslide occurred on the volcano's eastern flank.

We think that Hades crater formed from magma withdrawal and subsequent collapse of the conduit such as observed for Hawaiian pit craters [*Okubo and Martel*, 1998]. We conclude this because: (1) there was no unusually large explosive signal on the moored hydrophone record during Period V, and (2) the seafloor observations are consistent with a collapse versus an explosive event, as discussed above. Because the crater formation and the deep eruption overlap in time, it is tempting to suggest a relationship between the two, i.e., summit collapse from magma withdrawal coupled to down rift intrusion and eruption, as is well documented on subaerial volcanoes such as in Hawaii [*Epp et al*., 1983; *Decker*, 1987; *Tilling and Dvorak*, 1993] and on some submarine volcanoes [*Garcia et al*., 2006; *Chadwick et al*., 2012a]. In any case, the observational record for West Mata demonstrates that recent growth of the volcano has been by both summit and rift zone activity.

The PV East landslide may also have been associated with the magma withdrawal. A similar (but larger) landslide on NW Rota-1 seamount was interpreted by *Chadwick et al*. [2012b] to have been triggered by an unusually large intrusion/eruption. It is puzzling that the PV East landslide event did not appear as a distinct signal on the hydrophone record, particularly since the moored hydrophone was located only ~3 km to the south of the summit of West Mata. In any case, the PV East landslide occurred in the months following the period of continuous eruptions from the summit. It was likely triggered by some combination of long-term loading, stresses induced during magma withdrawal and crater formation (the crater rim and the headwall of the slide are only separated in distance by ~75 m), and/or regional tectonic earthquakes.

7.2. Relationship of Activity of West Mata to 2009 Earthquakes?

Bohnenstiehl et al. [2013a] show that West Mata had a significant increase in hydroacoustic signal intensity following the $M_w = 8.1$ earthquake of 29 September 2009, which ruptured the outer rise of the Tonga Trench ~180 km to the east and triggered two large ($M_w = 7.8$) thrust events on the subduction interface; West Mata is located within the aftershock zone of the subduction events [*Lay et al*., 2010]. *Bohnenstiehl et al*. [2013a] show that a months-long increase in hydroacoustic output of West Mata (recorded on an acoustic array ~600 km south of the volcano) was initiated at the time of the September 2009 earthquakes. They proposed that the gas-driven eruptions such as observed at West Mata in May 2009 intensified because of enhanced exsolution of magmatic gas due to a change in the dynamic stress field induced by the earthquake and its aftershocks. Increased volcanic activity has sometimes been observed on subaerial volcanoes after major earthquakes [*Hill et al*., 2002; *Moran et al*., 2004; *Manga and Brodsky*, 2006; *Walter and Amelung*, 2007]. This was a short-term trend because the summit eruptions at West Mata ceased ~15 months following the earthquake activity.

7.3. Modes of Activity and Growth of West Mata

Clague et al. [2011] concluded that the volcano changed from an earlier mode when it was constructed primarily by rift zone eruptions to a more recent mode of summit construction, possibly following the formation of a small caldera. However, our study has located one probable eruption site on the deep WSWRZ during period I and two well-defined eruptive sites on or near the base of the WSWRZ during 2009–2011 (periods III–V), indicating that the recent growth history of the volcano is substantially more distributed in space and time. At least for the last 2 years of its activity, continuous summit activity was punctuated by eruptions on the WSWRZ. Volumetrically, rift zone eruptives, probably a mixture of lava flows and fragmental material, account for most of the volcaniclastic deposition during periods II–V. Volcaniclastic deposition from the summit vents is barely measurable with the bathymetric differencing method for this time interval. None of the CTDO tow-yos made in the 2008–2012 period (i.e., those few that sampled deeper water on the flanks of West Mata) detected hydrothermal signals deeper than ~1100 m, but this is not surprising given the short sampling window (hours) and limited spatial distribution of the CTDO casts and tows. The water column signal from the WSWRZ eruptions could easily have been missed, particularly if the eruptions were of relatively short duration compared to the chronic summit activity.

The discovery of the rift zone eruptions raises interesting questions about the magma plumbing system of West Mata. The large PIV + PV WSWRZ deep eruption is of particular interest because it is located beyond the current morphologic expression of the WSWRZ. Magma feeding the deep eruption could either have been from dike *injection*(s) beneath the summit area propagating along the WSW fracture system or from a melt zone directly below the eruption site. Static changes in the stress field might have played a role. For example, the September 2009 earthquakes and their aftershocks could have reactivated the underlying crustal fracture system of West Mata, increasing the likelihood of such an unusual eruption. In any case, we can conclude that the volcano continues to be constructed by both summit and rift zone activity at this stage of its geologic evolution.

The total volume of eruptives produced during the 1996–2012 period is at least 1.15×10^8 m^3 (0.115 km^3) (Table 2), somewhat higher than the 8.0×10^7 m^3 reported by *Clague et al*. [2011] because of the additional period analyzed. This is a minimum amount because of the detection limitations of the multibeam differencing technique. The approximate total volume of West Mata is ~ 32 km^3, so the ~16 year (1996–2012) historical period of West Mata documented in this study (using the conservative historical eruption rate) produced about 0.36% of the total volume of the volcano. At that rate, West Mata would have been constructed in ~4450 years. However, because volcanoes often have variable eruption rates through their history (e.g., higher rates during youth), a much longer period of observation and/or age dating of rocks from the interior of the volcano would be necessary to realistically estimate the growth history of this type of submarine volcano.

West Mata is one of only two sites on the planet (NW Rota-1 being the other example) where a deepwater eruption has been directly observed. Both sites have significantly advanced our understanding of submarine volcanism and, along with the record from a small number of other sites such as Axial Seamount and the EPR 9°N–10°N, have demonstrated the value of long time series at submarine volcanic systems.

Acknowledgments

Support for R.W.E. during this study was by internal NOAA funding to the NOAA Vents Program (now Earth-Ocean Interactions Program). The NSF Ridge 2000 and MARGINS programs played a major role in the planning and justification for the 2009 rapid response proposal that funded the May 2009 expedition. MBARI provided support and outstanding postprocessing of the multibeam bathymetry from the *D. Allan B*. AUV multibeam sonar used in this study. NSF also provided major funding for the 2009 expedition (OCE930025 and OCE-0934660 to JAR) and for the 210Po-210Pb radiometric dating (OCE-0929881 and for the 210Po-210Pb radiometric dating (OCE-0929881 to KHR)). The NOAA Office of Exploration and Research provided major funding for the 2009 and 2012 field programs. We are indebted to the Kingdom of Tonga for allowing us to work within their Exclusive Economic Zone. We also thank the crew and technical staff of the research vessels and science teams on the research cruises of the *T.G. Thompson*, *Kilo Moana*, and *Roger Revelle*. The *Jason* (WHOI) and *QUEST 4000* (MARUM, Universtiy of Bremen, Germany) ROV teams provided excellent at-sea support. We are grateful to Chief Scientist Fernando Martinez and Peter Crowhurst (Nautilus Minerals Inc.) for providing time for a multibeam survey of West Mata during cruise KM1129a (November 2011). Detailed information on the multibeam bathymetry data files and processing is in supporting information Table S1. Multibeam bathymetry data files in this paper are available using file names and link provided in supporting information Text S2 and Table S1. CTDO data used in this study are in supporting information Table S2. Helium isotope and Hydrogen data are in supporting information Table S3. Details of age dating of the boninite samples reported here are in supporting information Text S3 and Table S4 or from author K. Rubin (krubin@hawaii.edu). The data are available for download from the EarthChem library via doi:10.1594/IEDA/100444. Expedition reports for ROV dive programs in 2009, 2012, and some other expeditions can be downloaded at: http://www.pmel.noaa.gov/eoi/laubasin.html (cruise identifiers in Table 1). Hydrophone data used in this study are available on request from author R. Dziak (robert.p.dziak@noaa.gov). We thank D. J. Fornari, R. J. Stern, and A. S. Soule for their constructive reviews. PMEL contribution 4119, JISAO contribution 2160, and SOEST contribution 9176.

References

American Public Health Association (2007), *Standard Methods for the Examination of Water and Wastewater*, 16th ed., 1268 pp., Am. Public Health Assoc., Washington, D. C.

Baker, E. T., G. J. Massoth, C. E. J. de Ronde, J. E. Lupton, and B. I. A. McInnes (2002), Observations and sampling of an ongoing subsurface eruption of Kavachi volcano, Solomon Islands, May 2000, *Geology*, *30*(11), 975–978.

Baker, E. T., W. W. Chadwick Jr., J. P. Cowen, R. P. Dziak, K. H. Rubin, and D. J. Fornari (2012), Hydrothermal discharge during submarine eruptions: The importance of detection, response, and new technology, *Oceanography*, *25*(1), 128–141, doi:10.5670/oceanog.2012.11.

Baumberger, et al., (2014), Understanding a volcanic eruption through time series hydrothermal plume sampling of dissolved gases: West mata Volcano, 2008–2012, *Geochem. Geophys. Geosyst.*, 146–147.

Bohnenstiehl, D. R., R. P. Dziak, H. Matsumoto, and J. Conder (2013a), Acoustic response of submarine volcanoes in the Tofua arc and northern Lau basin to two great earthquakes, *Geophys. J. Int.*, *196*(3), 1657–1675, doi:10.1093/gji/ggt472.

Bohnenstiehl, D. R., R. P. Dziak, H. Matsumoto, and T.-K. Lau (2013b), Underwater acoustic records from the March 2009 eruption of Hunga Ha'apai–Hunga Tonga volcano in the Kingdom of Tonga, *J. Volcanol. Geotherm. Res.*, *249*, 12–24, doi:10.1016/j.jvolgeores.2012.08.014.

Caplan-Auerbach, J., R. P. Dziak, W. W. Chadwick, and T.-K. Lau (2014), Hydroacoustic investigation of submarine landslides at West Mata volcano, Lau Basin, *Geophys. Res. Lett.*, *41*, 5927–5934, doi:10.1002/2014GL060964.

Caress, D. W., D. A. Clague, J. B. Paduan, J. Martin, B. Dreyer, W. W. Chadwick Jr., A. Denny, and D. S. Kelley (2012), Repeat bathymetric surveys at 1-metre resolution of lava flows erupted at Axial Seamount in April 2011, *Nat. Geosci.*, *5*(7), 483–488, doi:10.1038/ngeo1496.

Chadwick, W. W., Jr., R. W. Embley, and C. G. Fox (1991), Evidence for volcanic eruption on the southern Juan de Fuca ridge between 1981 and 1987, *Nature*, *350*(B3), 416–418.

Chadwick, W. W., Jr., I. C. Wright, U. Schwarz-schampera, O. Hyvernaud, D. Reymond, and C. E. J. de Ronde (2008a), Cyclic eruptions and sector collapses at Monowai submarine volcano, Kermadec arc: 1998–2007, *Geochem. Geophys. Geosyst.*, *9*, Q10014, doi:10.1029/2008GC002113.

Chadwick, W. W., Jr., K. V. Cashman, R. W. Embley, R. P. Dziak, C. E. J. de Ronde, H. Matsumoto, N. Deardorff, and S. G. Merle (2008b), Direct video and hydrophone observations of submarine explosive eruptions at NW Rota-1 volcano, Mariana Arc, *J. Geophys. Res.*, *113*, B08S10, doi:10.1029/2007JB005215.

Chadwick, W. W., Jr., S. L. Nooner, D. A. Butterfield, and M. D. Lilley (2012a), Seafloor deformation and forecasts of the April 2011 eruption at Axial Seamount, *Nat. Geosci.*, *5*(7), 474–477, doi:10.1038/ngeo1464.

Chadwick, W. W., Jr., R. P. Dziak, J. H. Haxel, R. W. Embley, and H. Matsumoto (2012b), Submarine landslide triggered by volcanic eruption recorded by in situ hydrophone, *Geology*, *40*(1), 51–54, doi:10.1130/G32495.1.

Clague, D. A., J. B. Paduan, and A. S. Davis (2009), Widespread strombolian eruptions of mid-ocean ridge basalt, *J. Volanol. Geotherm. Res.*, *180*(2–4), 71–188, doi:10.1016/j.jvolgeores.2008.08.007.

Clague, D. A., J. B. Paduan, D. W. Caress, H. Thomas, W. W. Chadwick Jr., and S. G. Merle (2011), Volcanic morphology of West Mata Volcano, NE Lau Basin, based on high-resolution bathymetry and depth changes, *Geochem. Geophys. Geosyst.*, *12*, QOAF03, doi:10.1029/2011GC003791.

Decker, R. W. (1987), Dynamics of Hawaiian volcanoes, in *Volcanism in Hawaii, U.S. Geol. Surv. Prof. Pap. 1350*, vol. 2, edited by R. W. Decker, T. L. Wright, and P. H. Stauffer, pp. 997–1018, U. S. Gov. Print. Off., Washington, D. C.

Dziak, R. P., R. W. Embley, E. T. Baker, W. W. Chadwick, J. A. Resing, H. Matsumoto, J. H. Haxel, S. L. Walker, and D. R. Bohnenstiehl (2009), Long-term explosion records from two erupting submarine volcanoes in the Mariana and Tonga island-arcs, *Eos Trans. AGU*, *90*(52), Fall Meet. Suppl., Abstract V44B-02.

Dziak, R. P., D. R. Bohnenstiehl, E. T. Baker, H. Matsumoto, J. H. Haxel, S. L. Walker, and M. J. Fowler (2010), Volcanic explosions, seismicity, and debris from the West and North Mata volcano complex, NE Lau Basin, Abstract V44B-02 presented at Fall Meeting, AGU, San Francisco, Calif., 13–17 Dec.

Dziak, R. P., D. R. Bohnenstiehl, and D. K. Smith (2012), Hydroacoustic monitoring of oceanic spreading centers: Past, present, and future, *Oceanography*, *25*(1), 116–127, doi:10.5670/oceanog.2012.10.

Dziak, R. P., D. Bohnenstiehl, E. Baker, H. Matsumoto, J. Caplan-Auerbach, C. Mack, R. Embley, S. Merle, and T.-K. Lau (2013), Acoustic and tephra records of explosive eruptions at West Mata submarine volcano, NE Lau Basin, Abstract V21C-2733 presented at 2013 Fall Meeting, AGU, San Francisco, Calif., 9–13 Dec.

Embley, R. W., et al. (2006), Long-term eruptive activity at a submarine arc volcano, *Nature*, *441*, 494–497, doi:10.1038/nature04762.

Embley, R. W., S. G. Merle, R. P. Dziak, K. H. Rubin, F. Martinez, and P. V. Crowhurst (2012), Pit crater formation and mass-wasting on West Mata volcano in 2010–2011 interpreted from repeat bathymetric surveys, Abstract T51D-2604 presented at 2012 Fall Meeting, AGU, San Francisco, Calif., 3–7 Dec.

Epp, D., R. W. Decker, and R. T. Okamura (1983), Relation of summit deformation to east rift zone eruptions on Kilauea Volcano, Hawaii, *Geophys. Res. Lett.*, *10*(7), 493–496.

Falloon, T. J., L. V. Danyushevsky, T. J. Crawford, R. Maas, J. D. Woodhead, S. M. Eggins, S. H. Bloomer, D. J. Wright, S. K. Zlobin, and A. R. Stacey (2007), Multiple mantle plume components involved in the petrogenesis of subduction-related lavas from the northern termination of the Tonga Arc and northern Lau Basin: Evidence from the geochemistry of arc and backarc submarine volcanics, *Geochem. Geophys. Geosyst.*, *8*, Q09003, doi:10.1029/2007GC001619.

Fornari, D. J., et al. (2012), The East Pacific Rise between 9 degrees N and 10 degrees N: Twenty-five years of integrated, multidisciplinary oceanic spreading center studies, *Oceanography*, *25*(1), 18–43, doi:10.5670/oceanog.2012.02.

Fox, C. G., W. W. Chadwick Jr., and R. W. Embley (1992), Detection of changes in ridge-crest morphology using repeated multibeam sonar surveys, *J. Geophys. Res.*, *97*(B7), 11,149–11,162.

Fox, C. G., H. Matsumoto, and T.-K. A. Lau (2001), Monitoring Pacific Ocean seismicity from an autonomous hydrophone array, *J. Geophys. Res.*, *106*(B3), 4183–4206.

Garcia, M. O., J. Caplan-Auerbach, E. H. De Carlos, M. D. Kurz, and N. Becker (2006), Geology, geochemistry and earthquake history of Loihi Seamount: Hawaii's youngest volcano, *Chem. Erde*, *66*, 81–108, doi:10.1016/j.chemer.2005.09.002.

Govers, R., and M. J. R. Wortel (2005), Lithosphere tearing at STEP faults: Response to edges of subduction zones, *Earth Planet. Sci. Lett.*, *236*(1–2), 505–523, doi:10.1016/j.epsl.2005.03.022.

Head, J. W., III, and L. Wilson (2003), Deep submarine pyroclastic eruptions: Theory and predicted landforms and deposits, *J. Volcanol. Geotherm. Res.*, *121*, 155–193.

Hill, D. P., F. Pollitz, and C. Newhall (2002), Earthquake-volcano interactions, *Phys. Today*, *55*(11), 41–47.

Johnson, R. H. (1973), Acoustic observations of nonexplosive submarine volcanism, *J. Geophys. Res.*, *78*(26), 6093–6096.

Lay, L., C. J. Ammon, H. Kanamori, L. Rivera, K. D. Koper, and A. R. Hutko (2010), The 2009 Samoa-Tonga great earthquake triggered doublet, *Nat. Geosci.*, *466*, 964–968, doi:10.1038/nature09214.
Lilley, M. D., D. A. Butterfield, J. E. Lupton, and E. J. Olson (2003), Magmatic events can produce rapid changes in hydrothermal vent chemistry, *Nature*, *422*(6934), 878–881.
Lupton, J. E. (1990), Water-column hydrothermal plumes on the Juan de Fuca Ridge, *J. Geophys. Res.*, *95*(B8), 12,829–12,842.
Manga, M., and E. Brodsky (2006), Seismic triggering of eruptions in the far field: Volcanoes and geysers, *Annu. Rev. Earth Planet. Sci.*, *34*, 263–291, doi:10.1146/annurev.earth.34.031405.125125.
Matsumoto, H., S. E. Stalin, R. W. Embley, J. H. Haxel, D. R. Bohnenstiehl, R. P. Dziak, C. Meinig, J. A. Resing, and N. M. Delich (2010), Hydroacoustics of a submarine eruption in the northeast Lau Basin using an acoustic glider, in *Oceans 2010 MTS/IEEE*, IEEE, doi:10.1109/oceans.2010.5664494.
Matsumoto, H., D. R. Bohnenstiehl, J. H. Haxel, R. P. Dziak, and R. W. Embley (2011), Mapping the sound field of an erupting submarine volcano using an acoustic glider, *J. Acoust. Soc. Am.*, *129*(3), EL94–EL99, doi:10.1121/1.3547720.
Millen, D. W., and M. W. Hamburger (1998), Seismological evidence for tearing of the Pacific plate at the northern termination of the Tonga subduction zone, *Geology*, *26*(7), 659–662.
Moran, S. C., J. Caplan-Auerbach, J. A. Power, S. D. Stihler, and J. J. Sánchez (2004), Earthquake triggering at Alaskan volcanoes following the 3 November 2002 Denali fault earthquake, *Bull. Seismol. Soc. Am.*, *94*(6), suppl. B, S300–S309, doi:10.1785/0120040608.
Norris, R. A., and R. H. Johnson (1969), Submarine volcanic eruptions recently located in the Pacific by Sofar hydrophones, *J. Geophys. Res.*, *74*(2), 650–664.
Okubo, C. H., and S. J. Martel (1998), Pit crater formation on Kilauea volcano, Hawaii, *J. Volcanol. Geotherm. Res.*, *86*(1–4), 1–18.
Resing, J. A., E. T. Baker, J. E. Lupton, S. L. Walker, D. A. Butterfield, G. J. Massoth, and K. Nakamura (2009), Chemistry of hydrothermal plumes above submarine volcanoes of the Mariana Arc, *Geochem. Geophys. Geosyst.*, *10*, Q02009, doi:10.1029/2008GC002141.
Resing, J. A., et al. (2011), Active submarine eruption of boninite in the northeastern Lau Basin, *Nat. Geosci.*, *4*, 799–806, doi:10.1038/ngeo1275.
Resing, J. A., R. W. Embley, and S. G. Merle (2012), Submarine ring of Fire-2012 (SRoF-12) Northest Lau Basin, R/V Roger Revelle Expedition RR1211, Cruise Report. [Available at http://oceanexplorer.noaa.gov/explorations/12fire/logs/summary/srof12-cruisereport-final.pdf.]
Rubin, K. H., and R. W. Embley (2012), Identification and implications of a submarine monogenetic field in the NE Lau Basin, Abstract T51D-2605 presented at 2012 Fall Meeting, AGU, San Francisco, Calif., 3–7 Dec.
Rubin, K. H., J. D. Macdougall, and M. R. Perfit (1994), ^{210}Po-^{210}Pb dating of recent volcanic eruptions on the sea floor, *Nature*, *368*, 841–844.
Rubin, K. H., M. Tolstoy, D. J. Fornari, R. P. Dziak, S. A. Soule, F. Waldhauser, and K. L. V. Damm (2008), Integrating radiometric, geophysical and thermal signals of volcanic unrest and eruption in 2005–06 at 9°50′N EPR, *Eos Trans. AGU*, *89*(53), Fall Meet. Suppl., Abstract V43I-07.
Rubin, K. H., S. A. Soule, W. W. Chadwick Jr., D. J. Fornari, D. A. Clague, R. W. Embley, E. T. Baker, M. R. Perfit, D. W. Caress, and R. P. Dziak (2012), Volcanic eruptions in the deep sea, *Oceanography*, *25*(1), 142–157, doi:10.5670/oceanog.2012.12.
Sansone, F. J., J. A. Resing, G. W. Tribble, P. N. Sedwick, K. M. Kelly, and K. Hon (1991), Lava-seawater interactions at shallow-water submarine lava flows, *Geophys. Res. Lett.*, *18*(9), 1731–1734.
Staudigel, H., and D. Clague (2010), The geological history of deep-sea volcanoes: Biosphere, hydrosphere, and lithosphere Interactions, *Oceanography*, *23*(1), 59–71, doi:10.5670/oceanog.2010.62.
Tilling, R. I., and J. J. Dvorak (1993), Anatomy of a basaltic volcano, *Nature*, *363*, 125–133.
Walker, S. L., E. T. Baker, J. A. Resing, K. Nakamura, and P. D. McLain (2007), A new tool for detecting hydrothermal plumes: An ORP sensor for the PMEL MAPR, *Eos Trans. AGU*, *88*(52), Fall Meet. Suppl., Abstract V21D-0753.
Walker, S. L., E. T. Baker, J. A. Resing, W. W. Chadwick Jr., G. T. Lebon, J. E. Lupton, and S. G. Merle (2008), Eruption-fed particle plumes and volcaniclastic deposits at a submarine volcano: NW Rota-1, Mariana Arc, *J. Geophys. Res.*, *113*, B08S11, doi:10.1029/2007JB005441.
Walker, S. L., E. T. Baker, J. E. Lupton, J. A. Resing, P. V. Crowhurst, R. Greene, and N. Buck (2009), Near and far field particle plumes around an erupting volcano—W Mata, NE Lau Basin, *Eos Trans. AGU*, *90*(52), Fall Meet. Suppl., Abstract V51D-1717.
Walker, S. L., E. T. Baker, M. I. Leybourne, C. E. J. de Ronde, R. Greene, K. Faure, W. W. Chadwick, R. P. Dziak, J. E. Lupton, and G. Lebon (2010), Transport of fine ash through the water column at erupting volcanoes—Monowai cone, Kermadec-Tonga Arc, Abstract T13B-2193 presented at 2010 Fall Meeting, AGU, San Francisco, Calif., 13–17 Dec.
Walter, T. R., and F. Amelung (2007), Volcanic eruptions following M $\geq$ 9 megathrust earthquakes: Implications for the Sumatra-Andaman volcanoes, *Geology*, *35*, 539–542, doi:10.1130/G23429A.1.
Watts, A. B., C. Peirce, I. Grevemeyer, M. Paulatto, W. Stratford, D. Bassett, J. A. Hunter, L. M. Kalnins, and C. E. J. de Ronde (2012), Rapid rates of growth and collapse of Monowai submarine volcano, Kermadec Arc, *Nat. Geosci.*, *5*, 510–515, doi:10.1038/ngeo1473.
Wright, I. C., W. W. Chadwick Jr., C. E. J. D. Ronde, D. Reymond, O. Hyvernaud, H.-H. Gennerich, P. Stoffers, K. Mackay, M. Dunkin, and S. C. Bannister (2008), Collapse and reconstruction of Monowai submarine volcano, Kermadec arc, 1998–2004, *J. Geophys. Res.*, *113*, B08S03, doi:10.1029/2007JB005138.
Young, C., and J. E. Lupton (1983), An ultra-tight fluid sampling system using cold-welded copper tubing, *Eos Trans. AGU*, *64*, 735.